

# Divergence in climate model projections of Arctic Atlantification

Morven Muilwijk,<sup>a,b</sup> Aleksi Nummelin,<sup>c</sup> Céline Heuzé,<sup>d</sup> Igor V. Polyakov,<sup>e</sup> Hannah Zanowski,<sup>f</sup>  
and Lars H. Smedsrud,<sup>b</sup>

<sup>a</sup> *Norwegian Polar Institute, Tromsø, Norway*

<sup>b</sup> *Geophysical Institute, University of Bergen and Bjerknes Centre for Climate Research, Bergen,  
Norway*

<sup>c</sup> *Norwegian Research Centre and Bjerknes Centre for Climate Research, Bergen, Norway*

<sup>d</sup> *Department of Earth Sciences, University of Gothenburg, Gothenburg, Sweden*

<sup>e</sup> *International Arctic Research Center and College of Natural Sciences and Mathematics,  
University of Alaska Fairbanks, Fairbanks, US*

<sup>f</sup> *Department of Atmospheric and Oceanic Sciences, University of Wisconsin-Madison, Madison,  
US*

This manuscript has been submitted for publication in Journal of Climate and is currently undergoing peer-review. Subsequent versions of this manuscript may have different content. If accepted, the final version of this manuscript will be available via the "Peer-reviewed publication DOI" link on the right-hand side of this page and will be available under open-access on the publisher's website.

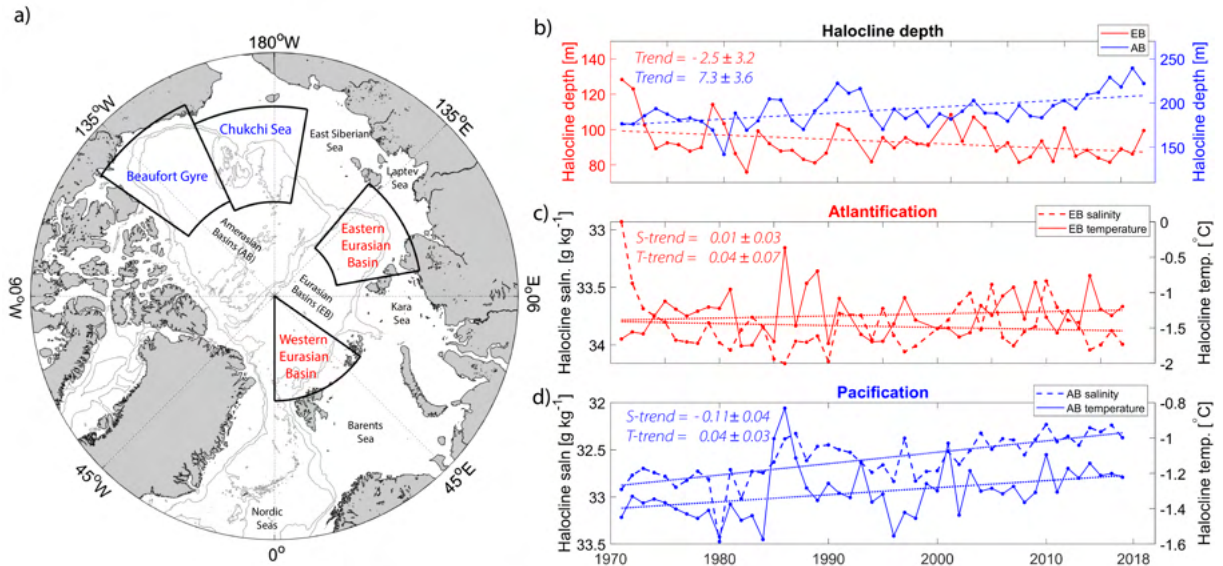
For any questions, contact the lead author Morven Muilwijk

14 ABSTRACT: The Arctic Ocean is strongly stratified by salinity in the uppermost layers. This  
15 stratification is a key attribute of the region as it acts as an effective barrier for the vertical ex-  
16 changes of Atlantic Water heat, nutrients, and CO<sub>2</sub> between intermediate depths and the surface  
17 of the Eurasian and Amerasian basins (EB and AB). Observations show that from 1970 to 2017,  
18 the stratification in the AB has strengthened, whereas, in parts of the EB, the stratification has  
19 weakened. The strengthening in the AB is linked to freshening and deepening of the halocline.  
20 In the EB, the weakened stratification is associated with salinification and shoaling of the halo-  
21 cline (Atlantification). Simulations from a suite of CMIP6 models project that, under a strong  
22 greenhouse-gas forcing scenario (ssp585), the overall surface freshening and warming continue in  
23 both basins, but there is a divergence in hydrographic trends in certain regions. Within the AB,  
24 there is agreement among the models that the upper layers will become more stratified. However,  
25 within the EB, models diverge regarding future stratification. This is due to different balances be-  
26 tween trends at the surface and trends at depth, related to Fram Strait fluxes. The divergence affects  
27 projections of future state of Arctic sea ice, as models with the strongest Atlantification project  
28 the strongest decline in sea ice volume in the EB. From these simulations, one could conclude  
29 that Atlantificaton will not spread eastward into the AB; however, we need to improve models to  
30 simulate tendencies in a more delicately stratified EB correctly.

## 31 **1. Introduction**

32 Much of the present-day central Arctic Ocean is a so-called beta ocean - it is strongly stratified by  
33 salinity, unlike subtropical seas where the upper layers are stratified by temperature (Nansen 1902;  
34 Carmack 2007). Over the last few decades, the Arctic region has experienced surface warming at  
35 more than twice the global rate (Cohen et al. 2020; IPCC 2021), and an intensive loss of Arctic sea  
36 ice and glacial ice (Stroeve and Notz 2018; Shepherd et al. 2020). These changes are associated with  
37 increased freshwater fluxes into the upper ocean (Solomon et al. 2021, and references therein), and  
38 changes in the intermediate and deeper layers (Årthun and Eldevik 2016). Even if the increasing  
39 trend in freshwater input to the Arctic Ocean is projected to continue (Zanowski et al. 2021), a  
40 stronger subpolar influence (borealization; Polyakov et al. 2020a) and the simultaneous loss of  
41 sea ice (Notz and SIMIP Community 2020) make the expected stratification changes non-trivial.  
42 Here, we aim to provide an overview of the changing Arctic stratification using unique historical  
43 observations and a range of future model projections.

44 Typically, the upper part of the water column in the deep Arctic basins (Eurasian Basin and  
45 Amerasian Basin, EB, and AB) is characterized by two distinct layers: a fresh and cold surface  
46 layer and a warmer and saline layer at depth with water of Atlantic origin (Rudels 2015). There is  
47 a cold halocline between them where the salinity increases rapidly with depth. This stratification  
48 is one of the essential attributes of the Arctic Ocean, acting as an effective barrier for water mass  
49 mixing and hence vertical exchanges (Peralta-Ferriz and Woodgate 2015). The strong layering  
50 effectively shields the sea ice cover from oceanic heat found at depth (Nansen 1902; Aagaard  
51 et al. 1981), limits primary production due to reduced nutrient fluxes (Randelhoff et al. 2020), and  
52 reduces the ocean's capability to take up atmospheric CO<sub>2</sub> (Yasunaka et al. 2018). The warm and  
53 saline Atlantic Water (AW) at intermediate depth enters the central Arctic Ocean via the deep Fram  
54 Strait and the shallow Barents Sea and circulates cyclonically in the Arctic interior, controlled  
55 by topography (Timmermans and Marshall 2020; Bluhm et al. 2020). The Atlantic inflow is the  
56 primary heat source for the Arctic Ocean, although Pacific Water (PW) is an important source  
57 of oceanic heat and relatively fresh water in the Pacific sector, especially in summer (Woodgate  
58 et al. 2012). The PW contributes to the low salinity in the uppermost layer (~ 250 m) of the AB  
59 (Proshutinsky et al. 2009, 2019). In contrast, in other Arctic regions, the major contributions of  
60 freshwater input to the Surface Mixed Layer (SML) stem from precipitation (Serreze et al. 2006),



65 FIG. 1. Arctic Ocean map with identified regions (a). Western Eurasian basin region, Eastern Eurasian basin  
 66 region, Chukchi Sea region, and Beaufort Gyre region are indicated. Light grey contour lines show the 500 m  
 67 and 2000 m isobaths from ETOPO1 bathymetry (Amante and Eakins 2009). Observed annual mean depth of  
 68 halocline base in the Eurasian basin (EB, red) and Amerasian basin (AB, blue) regions (b). Observed annual  
 69 mean temperature (solid line) and salinity (dashed line) averaged over the halocline layer in the EB region (c)  
 70 and AB region (d). Trend values are given per decade.

61 freshwater runoff from rivers (Holmes et al. 2012), glacial ice melting (Haine et al. 2015), and  
 62 melting of sea ice (Haine et al. 2015; Wang et al. 2019). The Arctic Ocean’s major outflows  
 63 carrying cold and fresh Polar Water (Timmermans and Marshall 2020) occur through the Canadian  
 64 Archipelago and the western part of Fram Strait.

71 The volume transport and temperature of AW entering the EB have increased (Tsubouchi et al.  
 72 2021; Smedsrud et al. 2022) and now play a greater role in sea ice loss in the Eurasian sector of  
 73 the Arctic (Carmack et al. 2015). Although the AW inflow historically has been significant for  
 74 regulating the sea ice cover in the Barents Sea and Western EB (Årthun et al. 2012; Onarheim  
 75 et al. 2015), its impact on sea ice has recently expanded towards the Eastern EB; a process often  
 76 referred to as “Atlantification” (Polyakov et al. 2017). Simultaneously, an anomalous advection of  
 77 warm and relatively fresh PW has been observed, resulting in a recent change called “Pacification”  
 78 (Polyakov et al. 2020a). The combined effect of both processes is referred to as a “Borealization”  
 79 (Polyakov et al. 2020a), a shift in the northward range and associated ecosystem of the Arctic

80 Ocean, which includes changes in both the physical, geochemical, and biological components.  
81 The hydrographic changes related to Atlantification and Pacification are expressed regionally  
82 and have opposite effects on stratification (Fig. 1 and Polyakov et al. 2020a). Pacification is  
83 mainly associated with the AB and an anomalous influx of PW. Generally, anomalous advection  
84 of PW sharpens the density gradient and results in a strengthened stratification in the AB (Steele  
85 2004). Atlantification has been manifested by a local surface layer salinification and, therefore, a  
86 weakening of the halocline and warming and shoaling of the AW layer below (Fig. 1 and Polyakov  
87 et al. 2020b). This results in an overall weakened stratification in the EB. These conditions are  
88 more susceptible to increased vertical mixing and thus favor biological production by bringing up  
89 nutrients (Polyakov et al. 2020a). Another essential local process is the general freshening of the  
90 upper EB and AB (Haine et al. 2015; Haine 2020; Solomon et al. 2021), which has resulted in  
91 a strengthened stratification (Li et al. 2020), especially in the AB (Polyakov et al. 2020a). The  
92 AB holds the largest reservoir of liquid freshwater in the Arctic, as the circulation in the Beaufort  
93 Gyre, sustained by the anticyclonic winds, drives Ekman convergence and deepens the halocline  
94 within the gyre (Proshutinsky 2002). Since the mid-1990s, hydrographic and satellite observations  
95 have shown increases and redistribution of freshwater in the Arctic (Rabe et al. 2011; Proshutinsky  
96 et al. 2019, and references therein). The increases have been linked to a combination of an  
97 intensification of the large-scale atmospheric forcing over the Beaufort Gyre (Giles et al. 2012;  
98 Proshutinsky et al. 2019; Cornish et al. 2020), increased river runoff (Peterson et al. 2002; Rabe  
99 et al. 2014; Haine et al. 2015), increased flux of freshwater through Bering Strait (Woodgate et al.  
100 2005) and direct contributions of sea ice melt (Wang et al. 2019). A recent review by Solomon  
101 et al. (2021) has, however, shown that the trend in total Arctic freshwater content in the 2010s has  
102 stabilized somewhat relative to the 2000s due to an increased compensation between a freshening  
103 of the Beaufort Gyre and a reduction in freshwater in the rest of the Arctic Ocean. Nonetheless,  
104 as the Arctic is expected to continue warming in response to emissions (Davy and Outten 2020),  
105 the freshwater fluxes into to the Arctic Ocean are projected to increase (e.g. Holland et al. 2007;  
106 Kattsov et al. 2007; Wang et al. 2021; Jahn and Laiho 2020; Zanowski et al. 2021), partly reflecting  
107 an intensification of the hydrological cycle (Held and Soden 2006; Haine 2020), and partly due to  
108 increased river runoff (Haine 2020). The freshwater flux due to melting sea ice has been a large  
109 contributor to the recent freshening, but is likely to decrease into the future, and become relatively

110 small by the second half of the 21st century, as less ice is available to melt (Shu et al. 2018).  
111 Experiments with column models (Nummelin et al. 2015; Davis et al. 2016) and a global climate  
112 model (Nummelin et al. 2016) have examined the potential effects of increased river runoff, and  
113 they find that the Arctic stratification will increase and that the freshwater has a larger effect than  
114 elevated wind-driven mixing (Davis et al. 2016). However, these studies do not consider other  
115 freshwater sources, the regional aspect, or the opposing effects of Atlantification. For example,  
116 using a single climate model (HiGEM), Lique et al. (2018) showed that under an extreme global  
117 warming scenario, the stratification in this model is strongly enhanced in the AB but reduced in  
118 the EB.

119 It is well known that climate models experience crucial biases in simulated Arctic hydrography.  
120 This is true for both ocean-sea-ice only models (Ilicak et al. 2016; Wang et al. 2016; Tsujino  
121 et al. 2020) and fully coupled climate models, such as the ones participating in the Climate  
122 Model Intercomparison Project phase 5 (CMIP5; Shu et al. 2019), and in the Climate Model  
123 Intercomparison Project phase 6 (Khosravi et al. 2022; Rosenblum et al. 2021, CMIP6). More  
124 specifically, the models struggle to represent AW circulation and mixing processes in the Central  
125 Arctic Ocean (Ilicak et al. 2016; Tsujino et al. 2020), have significant differences in circulation as a  
126 response to similar forcing (Mulwijk et al. 2019), and have a large spread in projections of sea ice  
127 cover (Shu et al. 2020). Despite these shortcomings, climate models are useful tools to investigate  
128 the competing processes mentioned above and evaluate how they will change into the future.

129 Khosravi et al. (2022) recently published an overview of biases in the Atlantic Water layer in the  
130 models that participated CMIP6. Their results indicate that biases persist from CMIP5 to CMIP6.  
131 Our companion paper, Heuzé et al. (2022), expanded on their results by also assessing the deep and  
132 bottom waters and by explaining the causes for all these biases, focusing primarily on the models'  
133 mean historical state. Additionally, Arctic freshwater storage and fluxes in a subset of the CMIP6  
134 models have been analyzed by Zanowski et al. (2021), and the sea ice in CMIP6 models has been  
135 assessed by Notz and SIMIP Community (2020) and Shen et al. (2021). Rosenblum et al. (2021)  
136 carefully examined one model (CESM2) in one region of the Arctic, but until now, no study has  
137 investigated hydrographic trends and stratification in multiple models and regions. We address  
138 this gap with a pan-Arctic examination of 14 CMIP6 models against the observations. Using a  
139 unique 48-year archive of observations (1970–2017), we first synthesize the observed changes in

140 different regions of the Arctic Ocean before comparing them to the historical simulations. We then  
141 describe how the stratification and hydrography in these regions are projected to change under a  
142 high (ssp585) emission scenario (O'Neill et al. 2016) and how this is related to changes in sea ice  
143 cover.

144 This manuscript is structured as follows: We start by describing the observational and model  
145 data used in this study and present a new diagnostic used to evaluate integral changes in Arctic  
146 Ocean stratification (Section 2). We then compare observed and simulated stratification in recent  
147 decades (Section 3a) before we investigate the future trends (Section 3b and 3c) and finally discuss  
148 the mechanisms responsible for these changes (Section 3d) and the impacts on sea ice (Section 3e).  
149 We focus particularly on the role of advective contra local processes and finish with a summary of  
150 our findings and a discussion on the broader implications of our work (Section 4).

## 151 **2. Data and Methods**

### 152 *a. Observational data*

153 This study uses a unique historical archive of hydrographic observations from 1970 to 2017,  
154 including Russian, American, Canadian and European ship and aircraft expeditions, year-round  
155 crewed drift stations, autonomous drifters, and submarine data. This is an updated version of the  
156 archive previously used by, e.g., Polyakov et al. (2020a) to investigate long-term AW variability  
157 and halocline stability, and has been made available through the Arctic Data Center (? , reference  
158 to appear latest during copy-editing). The temporal and spatial coverage for the data used in  
159 this study is shown in Fig. A1. Unfortunately, historical observations of the Arctic Ocean are  
160 generally sparse and have limited spatial coverage. Especially in the 1990s, data coverage is  
161 not good, and in general, there have been few winter campaigns in the central basins. However,  
162 autonomous Ice-Tethered Profilers (ITP), crewed ice-drift stations, and some ship-based campaigns  
163 ensure a relatively good seasonal coverage in later decades (Fig. A2). The bulk of historical data  
164 was gathered to construct the climatological atlases of the Arctic Ocean by Gorshkov (1980),  
165 Treshnikov (1985), and Timokhov and Tanis (1997). Before 1980 most observations used Nansen  
166 bottles to measure salinity, while modern and more accurate Conductivity-Temperature-Depth  
167 (CTD) instruments became more common as the use of icebreakers and submarines increased in  
168 the 1980s and 1990s. The typical accuracy of measurements from the Nansen bottles was estimated

169 by Timokhov and Tanis (1997) to be 0.01 °C for temperature and 0.02 for salinity. Since the 2000s, a  
170 major part of the data stems from ship-based measurements complemented by drifting ITPs, which  
171 autonomously collect CTD profiles down to 800 m. For consistency and direct comparison with  
172 model data we present salinity and and temperature in practical salinity units (psu) and potential  
173 temperature. All analysis is based on annual mean profiles. We use the TEOS10 equation of state  
174 as implemented in the Gibbs-SeaWater (GSW) Oceanographic Toolbox (McDougall and Barker  
175 2011) to calculate density.

### 176 *b. The CMIP6 models*

177 We use the output from 14 fully coupled models that participated in the Climate Model Inter-  
178 comparison Project phase 6 (CMIP6, Eyring et al. 2016), listed in Table 1. For comparison, these  
179 models are the same as those used in our companion paper (Heuzé et al. 2022) and were selected  
180 from the 35 CMIP6 models used in Heuzé (2021) as representative of their family, for diversity in  
181 vertical grid types and after eliminating the ones with the poorest bathymetry. Typical horizontal  
182 model resolution is ~50 km in the Arctic (9 km for the highest resolution) and 50 levels or more  
183 in the vertical. No more than two models share the same ocean component with the same version  
184 (Table 1).

189 We evaluated the last 45 years of the historical run, i.e., January 1970 – December 2014, and the  
191 first 85 years of the future high (ssp585) emission scenario (Eyring et al. 2016), i.e., January 2015  
192 – December 2100. The strong forcing scenario was chosen to clearly isolate climate change signals  
193 from internal variability. Trends were calculated from 1970–2014 to match the observational data  
194 and over 2015–2070 for the future scenario. Trends are not calculated over the full future period  
195 because the changes we observe are transient, and there is some flattening towards the end of the  
196 century (Section 3b). For the sea ice analysis presented in section 3e, the trends are calculated over  
197 the 2015–2045 period. For each model, only one ensemble member was used: ‘r1i1p1f1’ for the  
198 majority of models; ‘r1i1p1f2’ when r1i1p1f1 was not available (GISS-E2-1-H and UKESM1-0-  
199 LL). The simulated internal variability is not investigated in detail, and we note that under the high  
200 forcing scenario this is less important, whereas for the 1970–2014 period, forcing is modest and  
201 internal variability could play an important role. All trends presented are statistically significant  
202 unless otherwise stated. The output we used are the monthly seawater practical salinity “so”,



185 TABLE 1. Characteristics of the 14 CMIP6 models used in this study: horizontal grid type, horizontal resolution  
 186 in the Arctic, type of vertical grid and number of vertical levels, ocean model component, parameter used to  
 187 calculate sea ice volume, and reference. The horizontal resolution in the Arctic (3rd column) was calculated as  
 188 the square root of the total area north of 70°N divided by the number of points the model has north of 70°N. For  
 189 the vertical grids,  $\rho$  means isopycnic;  $\sigma$  terrain-following; and multiple symbols, hybrid.

Model	Grid type	Resolution	Vertical grid	Ocean model	Ice parameter	Reference
BCC-CSM2-MR	Tripolar	54 km	$z$ 40	MOM4-L40v2	sivol	Wu et al. (2019)
CAMS-CSM1-0	Tripolar	54 km	$z$ 50	MOM41	sivol	Xin-Yao et al. (2019)
CanESM5	Tripolar	50 km	$z$ 45	NEMO3.4.1	simass	Swart et al. (2019)
CESM2	Rotated	41 km	$z$ 60	POP2	sithick	Danabasoglu et al. (2020)
EC-Earth3	Tripolar	49 km	$z^*$ 75	NEMO3.6	sithick	Döscher et al. (2021)
GFDL-CM4	Tripolar	9 km	$\rho$ - $z^*$ 75	MOM6	sivol	Adcroft et al. (2019)
GFDL-ESM4	Tripolar	18 km	$\rho$ - $z^*$ 75	MOM6	sivol	Dunne et al. (2020)
GISS-E2-1-H	Regular	46 km	$\rho$ - $z$ - $\sigma$ 32	Hycom	sivol	Kelley et al. (2020)
IPSL-CM6A-LR	Tripolar	49 km	$z^*$ 75	NEMO3.2	sivol	Lurton et al. (2020)
MIROC6	Tripolar	39 km	$z$ - $\sigma$ 62	COCO4.9	sivol	Tatebe et al. (2019)
MPI-ESM1-2-HR	Tripolar	36 km	$z$ 40	MPIOM1.63	sivol	Müller et al. (2018)
MRI-ESM2-0	Tripolar	39 km	$z^*$ 60	MRI.COMv4	sivol	Yukimoto et al. (2019)
NorESM2-LM	Tripolar	38 km	$\rho$ - $z$ 53	BLOM (MICOM)	sivol	Seland et al. (2020)
UKESM1-0-LL	Tripolar	50 km	$z^*$ 75	NEMO3.6	sivol	Sellar et al. (2020)

203 potential temperature “thetao”, and sea ice concentration “siconc” and thickness “sivol/sithick” or  
 204 sea ice mass “simass” (Table 1). Water density was calculated using the TEOS10 equation of state  
 205 as implemented in the Gibbs-SeaWater (GSW) Oceanographic Toolbox (McDougall and Barker  
 206 2011). All computations were performed on the models’ native grid before being averaged for each  
 207 of the four regions shown in Fig. 1.

### 208 *c. Methods*

209 The primary objective of this paper is to quantify trends in stratification. Traditionally, strat-  
 210 ification has been quantified using the Brunt-Väisälä buoyancy frequency  $N^2 = -(g/\rho_0)\delta\rho/\delta z$ ,  
 211 where  $\rho$  is potential density,  $\rho_0$  is a reference density, and  $g$  is the gravitational acceleration. This  
 212 parameter provides a profile of stability between points in the vertical but does not yield a bulk  
 213 measure of the stability within a layer (Polyakov et al. 2018). The upper part of the EB and AB  
 214 water column features complex layering. It consists of a surface mixed layer (SML,  $\sim 20$ –50 m)

215 overlaying the halocline, characterized by cold temperatures and a very high salinity gradient ( $\sim$   
 216 50–250 m), and a warmer (temperature  $> 0^\circ\text{C}$ ) and more saline layer of AW below (Rudels et al.  
 217 2004). Traditionally, the definition of AW is based on temperature, salinity, or density values.  
 218 However, since we expect these properties to be biased in the models, we instead chose to define  
 219 the AW core as the depth of the temperature maximum below 100 m. When we further refer to  
 220 AW properties, we thus refer to the properties at the depth of the AW core. According to Heuzé  
 221 et al. (2022), the CMIP6 multi-model mean AW core depth is approximately 400 m in the EB and  
 222 approximately 530 m in the AB but varies substantially from model to model (ranging between 77  
 223 m and 1300 m).

224 The halocline is often divided into a cold halocline, with near-freezing temperatures, and lower  
 225 halocline waters, with increasing temperature and salinity with depth (Steele et al. 1989; Rudels  
 226 et al. 2004). Polyakov et al. (2018) noted that, especially within the halocline, which consists of  
 227 a complex combination of water masses with varying effects on stratification (Bluhm et al. 2015),  
 228  $N^2$  is insufficient as a measure of stratification since it does not provide a bulk metric. Also, a  
 229 simple density contrast between two levels ( $\Delta\sigma_\theta$ ) is similarly insufficient. Polyakov et al. (2018)  
 230 therefore proposed Available Potential Energy (APE) as a good integral indicator of changes in  
 231 stratification in the combined SML and halocline layer. For each profile, APE is calculated as:

$$APE = \int_{H_{halo}}^{surface} g(\rho - \rho_{halo})zdz, \quad (1)$$

232 where  $H_{halo}$  is the depth of the lower boundary of the halocline and  $\rho_{halo}$  is the potential density  
 233 at that lower boundary of the halocline.

234 In observations, the lower boundary of the halocline is usually determined using a density ratio  
 235 algorithm following the method proposed by Bourgain and Gascard (2011), which was also used  
 236 by e.g. Polyakov et al. (2018) and Metzner et al. (2020). Following Bourgain and Gascard (2011),  
 237 such density ratio is defined as

$$R_\rho = \left| \left( \alpha \frac{\delta\Theta}{\delta z} \right) / \left( \beta \frac{\delta S_A}{\delta z} \right) \right| \quad (2)$$

238 where  $\alpha$  is the thermal expansion coefficient,  $\beta$  is the haline contraction coefficient,  $\Theta$  is the  
 239 conservative temperature, and  $S_A$  is the absolute salinity. The lower boundary of the halocline

240  $H_{halo}$  is then defined as the depth where  $R_\rho$  exceeds the threshold of 0.05, which was determined  
241 empirically from observations in the Arctic (Bourgain and Gascard 2011).

242 Unfortunately, models struggle to reproduce the Arctic halocline properly (Nguyen et al. 2009),  
243 and large temperature and salinity biases in the Arctic Ocean (Heuzé et al. 2022) make it difficult  
244 to properly define the halocline using the same criteria as in the observations. Manually deriving  
245 model-specific definitions is not ideal either, as the biases might vary over time. We, therefore,  
246 find that the uncertainty of properly defining the “correct” halocline in CMIP6 models based on  
247 Equation (1) is too high and have chosen to investigate Arctic stratification in CMIP6 models using  
248 an indicator whose definition is less dependent on defining a halocline.

249 We therefore propose a new indicator of stratification strength,  $\Delta PE(H)$ . First, we define the  
250 potential energy of the water column following Tailleux (2009) as:

$$PE(H) = \int_H^{surface} g(z)\rho(z)zdz \quad (3)$$

251 where  $H$  is a chosen depth level. We then look at the difference in potential energy between the  
252 simulated stratified water column and a fully mixed water column, which reflects the energy needed  
253 to fully mix the water column from the surface to a given depth:

$$\Delta PE(H) = PE(H) - PE(H)_{mixed}. \quad (4)$$

254 Here,  $PE(H)_{mixed}$  is the potential energy of a completely mixed water column with a mean  
255 temperature and salinity down to depth  $H$ .  $\Delta PE(H)$  thus represents the potential energy energy  
256 stored in stratification, and as long as  $H$  is well below the typical halocline depth, APE and  $\Delta PE$   
257 should capture similar changes and be equally good indicators of stratification strength. However,  
258  $\Delta PE(H)$  is preferred in models as its definition is independent of temperature and salinity gradients.  
259 Throughout the paper we will refer to  $\Delta PE$  as stratification strength or potential energy stored in  
260 stratification. A comparison of APE and  $\Delta PE$  is given in Fig. A3. We use  $H = 300$  m (well below  
261 the halocline according to Heuzé et al. 2022), but have repeated the calculations with different  
262 values of  $H$ , and the qualitative results are not sensitive to this choice. We also note that  $\Delta PE$   
263 describes a process of irreversible mixing, whereas APE describes the difference to adiabatically  
264 rearranged minimum energy, which would be reversible.

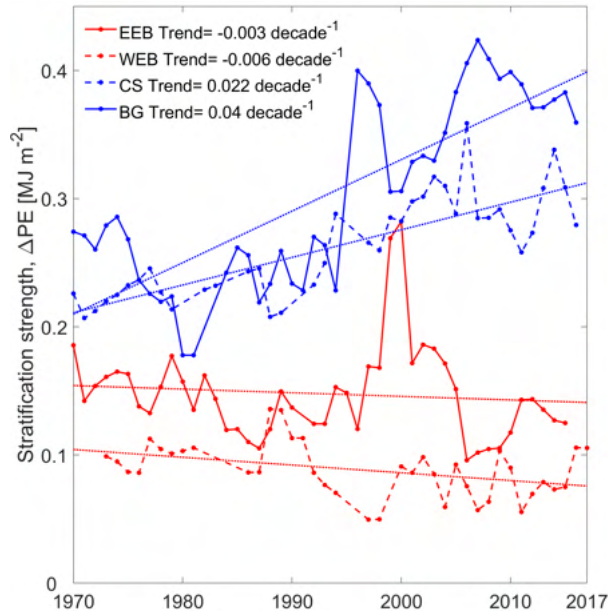
### 265 3. Results

#### 266 a. Recent decades (1970–2014)

##### 267 1) OBSERVED STRATIFICATION CHANGES

268 We start by analyzing hydrographic observations from four regions in the Arctic Ocean (Fig.  
269 1); two in the AB (Beaufort Gyre and the Chukchi Sea) and two in the EB (Western and Eastern  
270 EB), consistent with previous studies (e.g. Polyakov et al. 2020a). The halocline base is deeper in  
271 the AB ( $\sim 200$  m) than in the EB ( $\sim 90$  m, Fig. 1). Since 1970 it has deepened in the AB ( $\sim 7$   
272 m decade $^{-1}$ ) and shoaled in the EB ( $\sim 3$  m decade $^{-1}$ ), although the latter trend is not statistically  
273 significant. In the AB, the halocline freshens ( $\sim 0.11$  psu decade $^{-1}$ ), which other studies have  
274 documented (Carmack et al. 2016; Proshutinsky et al. 2019; Polyakov et al. 2020a). The EB  
275 halocline shows overall no statistically significant salinity trend, although a moderate salinification  
276 has been observed in the Eastern EB region in recent decades (Polyakov et al. 2020a, not shown  
277 here). The Eastern EB salinification and AB freshening were recently taken as indicators of the  
278 ongoing Atlantification and Pacification (Polyakov et al. 2020a), but we note that particularly  
279 Pacification is difficult to distinguish from the local freshening occurring in the upper Arctic Ocean  
280 due to increased runoff or precipitation. Alongside the halocline freshening in the AB, there is  
281 general warming ( $\sim 0.04$  °C decade $^{-1}$ ) related to PW inflow (Polyakov et al. 2020a). Also in the EB  
282 the halocline warms ( $\sim 0.04$  °C decade $^{-1}$ ), but again, these trends are not statistically significant.

287 The contrasting changes in upper ocean salinity and temperature in the EB and AB result in  
288 different effects on the regional halocline stability and thus stratification. In Fig. 2, we present the  
289 observed regional time series of potential energy stored in stratification. There is a strong positive  
290 trend in  $\Delta PE$  in the Chukchi Sea and Beaufort Gyre, which is associated with a strengthening of  
291 the stratification. In contrast, in the Western and Eastern EB, the  $\Delta PE$  shows a negative long-term  
292 trend, meaning the stratification is weakened (although much weaker trends than in the AB and  
293 not statistically significant in the Eastern EB). These findings are consistent with Polyakov et al.  
294 (2018) who showed that the most considerable changes in Arctic Ocean stratification have occurred  
295 in the AB and other studies which show that the halocline has weakened in the EB towards the  
296 end of the twentieth-century (Steele et al. 1989; Polyakov et al. 2017, 2020b). A comparison of  
297  $\Delta PE$  and APE, used in Polyakov et al. (2018) is shown in Fig. A3. Overall, the two metrics both

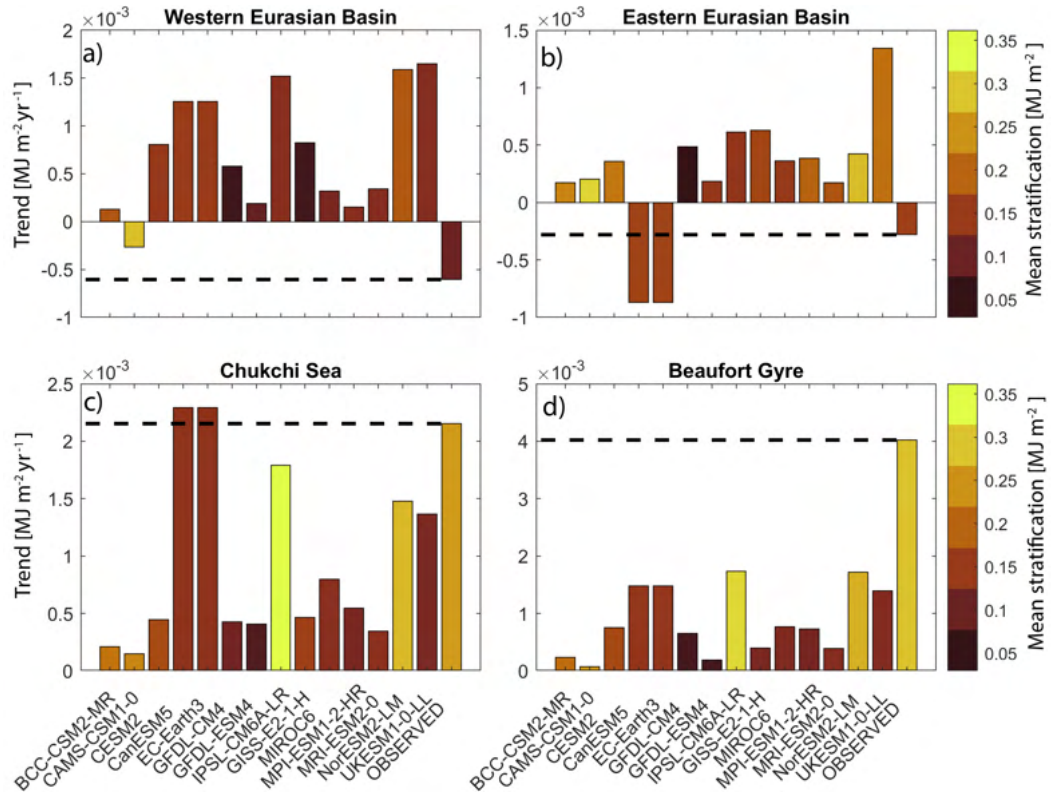


283 FIG. 2. Observed potential energy stored in stratification ( $\Delta PE(H)$ ) from 300 m following equation (4). Blue  
 284 colors are used for the AB, and red colors are used for EB. WEB = Western Eurasian basin, EEB = Eastern  
 285 Eurasian basin, CS = Chukchi Sea and BG = Beaufort Gyre. All trends, except the EEB, are statistically  
 286 significant.

298 show the opposite changes in the AB and EB, but  $\Delta PE$  includes changes in the AW just below the  
 299 halocline and therefore shows a stronger signal of Atlantification in the Western EB compared to  
 300 APE, which only takes into account changes to the bottom of the halocline. Clearly, the trends  
 301 are affected by how one chooses to represent stratification, and given their different definitions,  
 302 the metrics also show significant differences in internal variability. In the following section, we  
 303 compare the observed changes in stratification to simulations from 14 CMIP6 models.

## 304 2) SIMULATED STRATIFICATION CHANGES

305 In the AB, most models analyzed in this study are less stratified than observations (colors of bars  
 306 in Fig. 3), as also discussed by Heuzé et al. (2022) and Khosravi et al. (2022). Notable exceptions  
 307 are IPSL-CM6A-LR and NorESM2-LM. In the EB, most models are equally or more stratified than  
 308 observations, with GFDL-CM4 and GISS-E2-1-H as exceptions. In general, the models do not  
 309 correctly represent the difference in stratification between the two basins and instead have similar  
 310 values throughout the whole Arctic (i.e., the same color of bars on all panels of Fig. 3) – a result



316 FIG. 3. Simulated trends in stratification strength,  $\Delta PE$ , for each of the CMIP6 models listed in Table 1 from  
 317 1970–2014. Dashed black lines and rightmost bars indicate the observed trends (Fig. 2), and color bars indicate  
 318 the mean stratification strength in different regions for each model. Note the different y-axes on all panels.

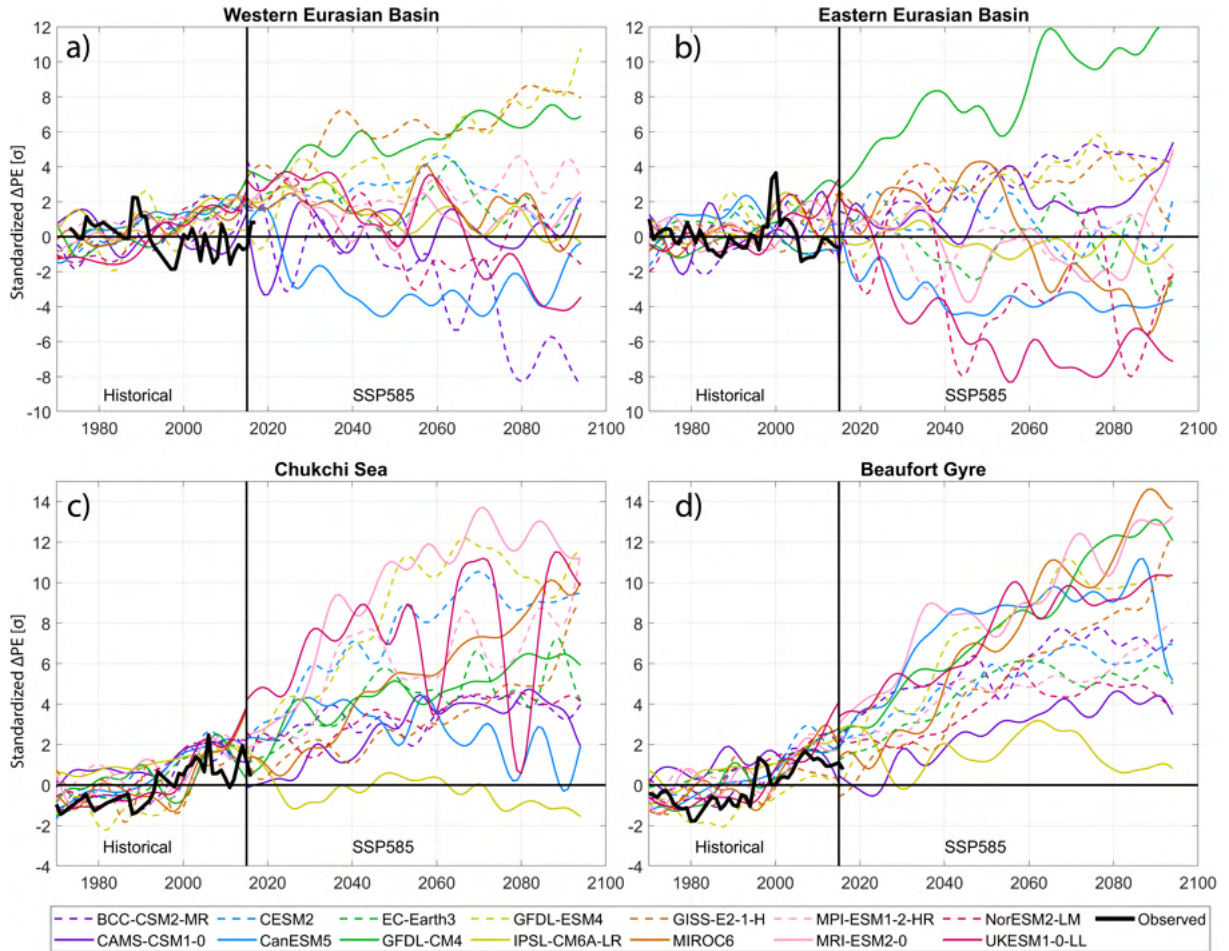
311 consistent with the biases in water mass properties described in Heuzé et al. (2022) and Khosravi  
 312 et al. (2022). In fact, several models are incorrectly more stratified in the EB than in the AB.  
 313 However, the biases in stratification are not consistent throughout the Arctic and vary from region  
 314 to region. It is worth noting that no model is too strongly biased to not be kept in this study, i.e.,  
 315 all stratification values are in the same order of magnitude as the observations.

319 In accordance with observations, all models show a positive trend in stratification (strengthening)  
 320 in the AB over the period 1970–2014 (Fig. 3, length of the bars). However, the absolute values  
 321 of the trends are much lower than in the observations. There appears to be no clear relationship  
 322 between the mean strength of stratification and the magnitude of trends (not shown). The models  
 323 also agree on a larger change in stratification in the AB compared to the EB, although they do not  
 324 show the opposite trends between the basins. In the Western EB, almost all models simulate a  
 325 strengthened stratification, and only CAM5-CSM1-0 produces a weakened stratification like the

326 observations. In the Eastern EB, there is a larger disagreement among the models, both in the mean  
327 state and in their trends, and here two models (CanESM5 and EC-Earth3) simulate a weakened  
328 stratification. In summary, only three models indicate an Atlantification (as diagnosed through  
329  $\Delta PE$ ) comparable to what has been observed. We emphasize here that we only investigate one  
330 ensemble member for each model, and that internal variability could have a significant impact  
331 on the trends during the 1970–2014 period where the external forcing is relatively weak. For  
332 example, experiments with a single model system (UKESM1-0-LL, not shown) show that among  
333 nine ensemble members, the trends in stratification in the Eastern EB (where the spread is largest)  
334 range between  $-0.0007 \text{ MJ m}^{-2} \text{ yr}^{-1}$  and  $+0.00117 \text{ MJ m}^{-2} \text{ yr}^{-1}$ . In the next sections, we investigate  
335 how the trends are projected to continue or change into the future under a strong greenhouse-gas  
336 forcing scenario.

### 337 *b. Future trends in stratification*

338 The temporal anomalies of the simulated potential energy stored in stratification,  $\Delta PE$  show  
339 significant variations in the various regions both in the historical period and under the ssp585  
340 forcing scenario (Fig. 4). Within the EB, the models diverge regarding future stratification. Fig  
341 4 shows large differences among the models, with the largest intermodel spread in the Eastern  
342 EB. Some models project a clear increase in EB stratification (e.g., GFDL-CM4, GFDL-ESM4,  
343 GISS-E2-1-H, and CAMS-CSM1-0) while others project a clear decrease (e.g., UKESM1-0-LL,  
344 CanESM5, NorESM2-LM, and IPSL-CM6A-LR). The future weakening of the EB stratification  
345 was also shown by Lique et al. (2018) using the HiGEM model. Despite only two models showing  
346 an indication of Atlantification in the period 1970–2014, approximately half of the models predict  
347 a future weakening of the EB stratification and thus Atlantification. Despite the large spread in  
348 the EB, there is agreement among the models (except IPSL-CM6A-LR, plain yellow line) on an  
349 increased future stratification in the Chukchi Sea and Beaufort Gyre regions. This means that the  
350 observed strengthening of the halocline in the AB is projected to continue and amplify into the  
351 future. In the Beaufort Gyre, the trends continue throughout the twenty-first century, whereas in the  
352 Chukchi Sea, the curve flattens in the 2060s for many of the models, albeit with strong interannual  
353 variability. This is likely related to the fact that at this point the region is practically ice-free for  
354 large portions of the year, and the freshwater contribution from sea ice melt therefore decreases.



360 FIG. 4. Regional time series (standardized anomalies relative to 1970–2014 mean) of stratification strength,  
 361  $\Delta PE$  [ $\text{MJ m}^{-2}$ ], for the 14 CMIP6 models listed in Table 1. More positive values means more energy is needed to  
 362 mix the water column. All time series are low-pass filtered with a five year cutoff-frequency. Note the different  
 363 y-axes for the two basins. For comparison, the observed stratification over the period 1970-2017 is plotted in  
 364 with thick black lines.

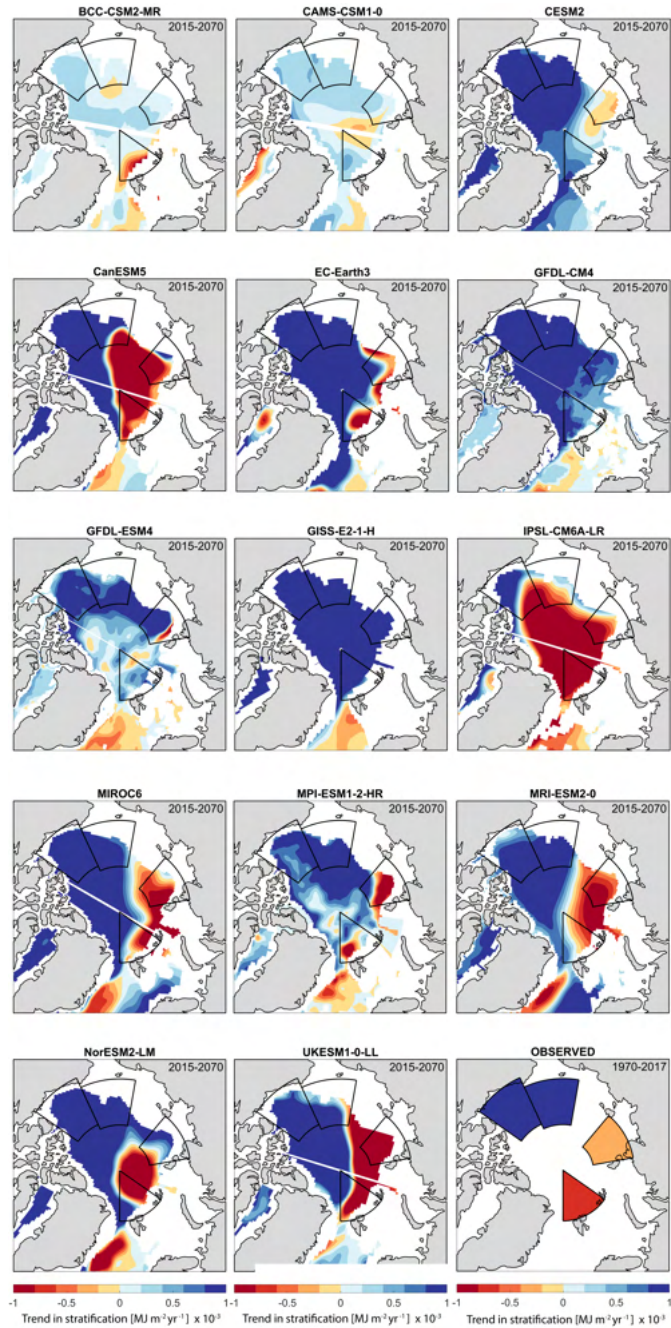
365 The freshwater input from river runoff is expected to continue to increase, but due to the prevailing  
 366 wind patterns in the region, most of this will accumulate in the Beaufort Gyre region and not stay  
 367 in the Chukchi Sea region. The future trends in the AB are comparable to the observed trend in  
 368 recent decades, but in the EB, both the trends and the interannual variations are amplified under  
 369 the strong forcing scenario.

369 The spatial extent of future trends in stratification varies significantly among the selected models,  
 370 but there are also some commonalities in the spatial patterns (Fig. 5). For example, there is a clear

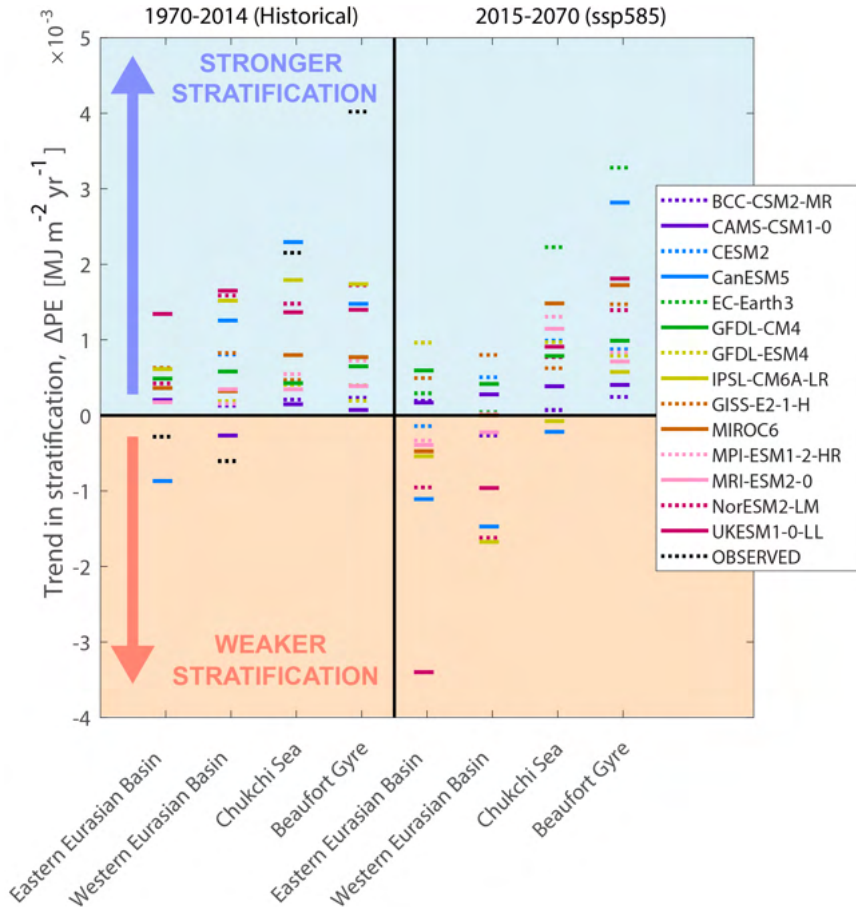


371 division and opposite trends in the AB and EB, similar to what has been documented by Polyakov  
372 et al. (2020a) and what can be seen from the lower right panel in Fig. 5. The opposing trends can  
373 be understood as the competing influences of the Atlantic and Arctic domains. All models show a  
374 weakening of stratification in some parts of the EB (red colors) and a strengthening of stratification  
375 in most parts of the AB (blue colors). However, the exact location, extent, and magnitude of the  
376 Atlantification signal varies, resulting in a large spread, especially in the Eastern EB. From Fig. 5  
377 we see that some of the discrepancies shown in Fig. 4 are strongly related to the spatial extent of the  
378 signals and the use of fixed regions. Interestingly, for most models, the indicated Atlantification is  
379 mainly confined towards the Eastern parts of the EB and the Barents Sea outflow near the St. Anna  
380 trough and less towards Fram Strait. It is possible that because AW is in closer contact with sea ice  
381 north of Svalbard, more sea ice is melted there, resulting in increased surface freshening and hence  
382 a strengthening of the stratification. GISS-E2-1-H is the only model that shows no indication of  
383 Atlantification, whereas IPSL-CM6A-LR, CanESM5, and UKESM1-0-LL show the largest spatial  
384 extent of Atlantic influence.

385 We quantify and summarize the historical and future trends for each region in Fig. 6. The  
386 dipole-like pattern is also clearly illustrated here, with obvious differences between the evolution  
387 of the EB and AB. The spread amongst the models is comparable in both basins ( $\sim 3 \text{ MJ m}^{-2} \text{ yr}^{-1}$ ),  
388 but this spread results in opposite signs in the EB, whereas, as shown previously, most models  
389 project an increase in stratification in the AB. Again, we note that some of these discrepancies  
390 reflect different spatial extent of the signals. The future trends in the AB are somewhat larger  
391 than the historical trends. More than half of the models show a strong weakening trend in the EB,  
392 with CanESM5, NorESM2-LM, IPSL-CM6A-LR, and UKESM1-0-LL having the largest changes.  
393 UKESM1-0-LL is an extreme in the Eastern EB with a trend four times stronger than any other  
394 model. These changes in stratification can be the result of changes in the upper ocean (SML and  
395 halocline) and water masses below the halocline, such as the AW. In the following section, we  
396 examine what drives the changes in stratification in the various regions and focus on the difference  
397 between the surface and AW layers.



365 FIG. 5. Future spatial trends in stratification strength,  $\Delta PE$ , under a strong greenhouse-gas forcing scenario  
 366 (ssp585) for the 14 CMIP6 models listed in Table 1. Negative values mean a weakening of stratification.  
 367 All trends are annual means calculated over the period 2015-2070. For comparison, the observed trends in  
 368 stratification over the period 1970-2017 is plotted in the last panel.



398 FIG. 6. Mean regional trends in stratification strength,  $\Delta PE$ , for our 14 CMIP6 models. The trends over the  
 399 historical period (1970-2014) are shown on the left, and the trends over the future period (2015-2070) under  
 400 a strong greenhouse-gas forcing scenario (ssp585) are shown on the right. As in Fig. 5, positive values (blue  
 401 shading) denote increased stratification, and negative values (orange shading) denote weakened stratification.  
 402 For comparison, the trends for the observations over the 1970–2017 period is shown by dashed black lines.

403 *c. Atlantic Water and surface trends*

404 We have now shown that the models diverge when predicting changes in stratification in the  
 405 EB and show a large spread in the AB. Khosravi et al. (2022) noted that "model biases in the  
 406 Arctic Ocean could have origins outside the Arctic Ocean and possibly in other components of  
 407 the climate system. Identifying these origins in individual models is needed to improve the Arctic  
 408 Ocean representation in CMIP simulations." In order to do so, we therefore focus on the water  
 409 masses that are the primary drivers for stratification change; the surface waters and the AW. We

419 TABLE 2. Future Atlantic Water core (temperature maximum below 100 m) temperature and salinity trends for  
 420 each of the CMIP6 models (forcing scenario ssp585) over 2015–2070. For comparison, the last row indicates the  
 421 trends for the observations over the 1970–2017 period. All values are given in °C decade<sup>-1</sup> and psu decade<sup>-1</sup>.  
 422 Statistically non-significant trends ( $p \geq 0.05$ ) are shown in italic.

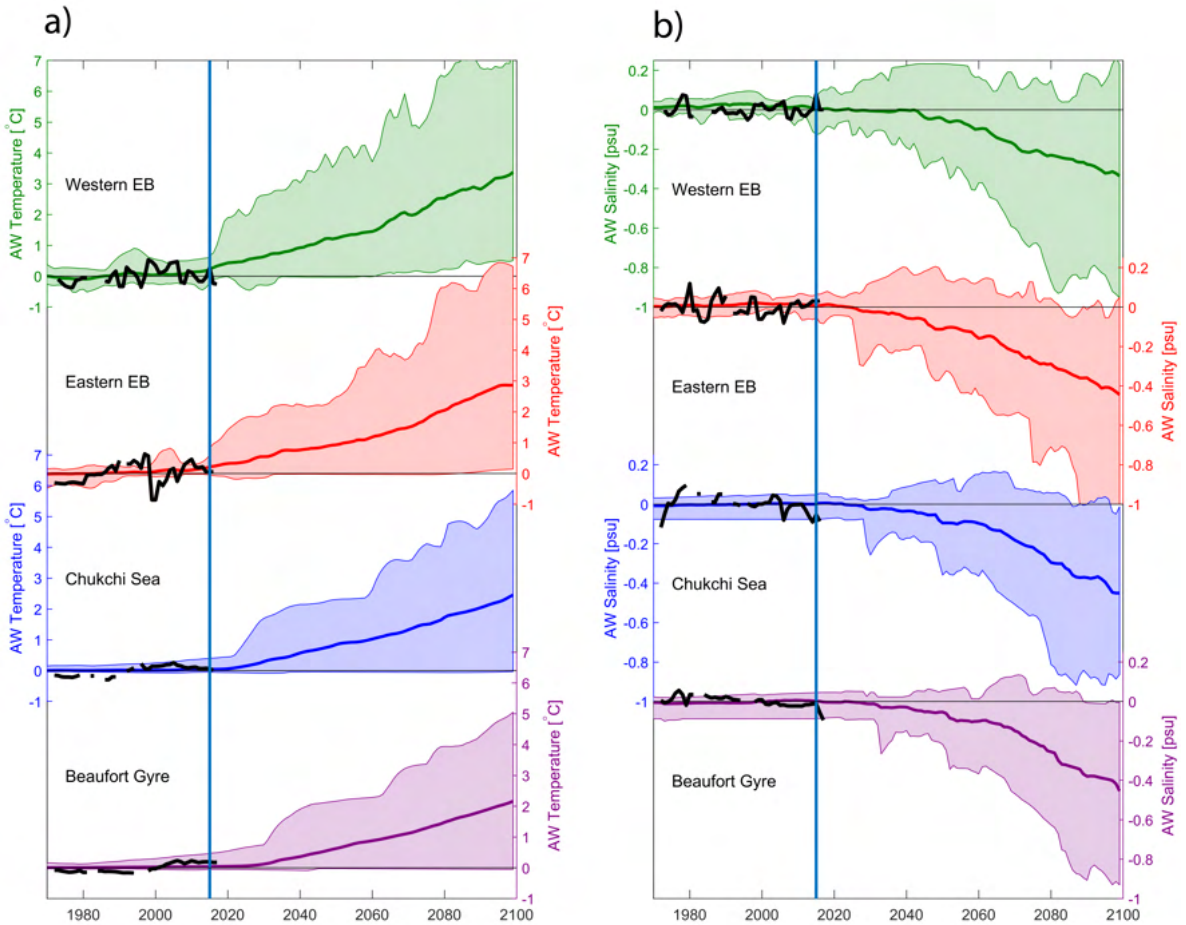
	Western EB		Eastern EB		Chukchi Sea		Beaufort Gyre	
	$\theta$	$S$	$\theta$	$S$	$\theta$	$S$	$\theta$	$S$
BCC-CSM2-MR	.013 ± .004	-.016 ± .005	-.002 ± .000	.003 ± .001	-.002 ± .000	-.004 ± .000	-.003 ± .000	-.004 ± .000
CAMS-CSM1-0	.032 ± .008	.015 ± .002	.012 ± .001	-.005 ± .001	.001 ± .001	-.015 ± .001	.006 ± .001	-.008 ± .002
CESM2	.355 ± .018	-.062 ± .007	.310 ± .013	-.047 ± .005	.224 ± .012	-.043 ± .002	.115 ± .010	-.045 ± .002
CanESM5	.729 ± .026	-.036 ± .004	.428 ± .021	-.082 ± .006	.454 ± .029	-.040 ± .006	.525 ± .029	-.017 ± .004
EC-Earth3	.606 ± .024	.028 ± .004	.470 ± .013	.011 ± .005	.429 ± .031	.056 ± .003	.225 ± .033	.041 ± .004
GFDL-CM4	.143 ± .005	-.021 ± .001	.120 ± .005	-.020 ± .002	.176 ± .010	-.009 ± .001	.088 ± .007	-.008 ± .001
GFDL-ESM4	.097 ± .018	-.032 ± .002	.152 ± .009	-.026 ± .001	.121 ± .008	-.024 ± .001	.061 ± .005	-.005 ± .001
IPSL-CM6A-LR	.402 ± .023	-.004 ± .005	.301 ± .021	-.018 ± .006	.330 ± .028	-.012 ± .007	.360 ± .023	-.020 ± .007
GISS-E2-1-H	.040 ± .007	.004 ± .007	.155 ± .008	.000 ± .005	.155 ± .002	-.009 ± .002	.125 ± .005	-.009 ± .002
MIROC6	.286 ± .019	-.092 ± .003	.122 ± .014	-.091 ± .003	.162 ± .004	-.072 ± .003	.144 ± .004	-.063 ± .004
MPI-ESM1-2-HR	.314 ± .016	-.015 ± .002	.105 ± .016	-.038 ± .002	.242 ± .019	-.016 ± .001	.301 ± .014	-.009 ± .001
MRI-ESM2-0	.444 ± .012	-.094 ± .004	.291 ± .013	-.093 ± .003	.268 ± .015	-.100 ± .003	.207 ± .016	-.092 ± .005
NorESM2-LM	.346 ± .017	-.063 ± .005	.171 ± .024	-.118 ± .005	.312 ± .020	-.096 ± .004	.299 ± .022	-.090 ± .005
UKESM1-0-LL	.740 ± .028	-.009 ± .005	.713 ± .024	-.038 ± .008	.735 ± .024	-.030 ± .008	.604 ± .036	-.035 ± .006
OBSERVED	.062 ± .030	-.0001 ± .004	.100 ± .034	-.000 ± .005	.087 ± .012	-.018 ± .005	.086 ± .008	-.014 ± .002

410 assume that most changes at the surface are driven by local processes (e.g., sea ice melt/growth,  
 411 river runoff, evaporation-precipitation, surface heat fluxes, etc.), and those in the AW layer are  
 412 primarily advected in through the Fram Strait and the Barents Sea, and mainly related to processes  
 413 beyond the boundaries of the Arctic Ocean. The question thus becomes: are the simulated changes  
 414 in stratification mainly locally driven or remotely forced? Of course, the layers are not fully  
 415 disconnected, and mixing occurs along the AW pathways, but Heuzé et al. (2022) revealed that in  
 416 the CMIP6 models, there is a strong decoupling between the upper layer and the rest of the deep  
 417 Arctic (below 200 m). This is partly attributed to an absence of ventilation, and as a result, the  
 418 properties of the Arctic AW layer are closely linked to the inflows.

423 We start by detailing the evolution of AW core temperature and salinity in the four different  
 424 regions. As expected, with continued global warming, the AW temperature is projected to increase  
 425 in all regions by all models (Fig. 7). Thick lines in Fig. 7 represent the multimodel mean  
 426 anomalies relative to each model’s historical mean, and colored envelopes indicate the minimum

427 and maximum of the model spread per time step. A full overview of the property trends in the  
428 various models is presented in Table 2. We note that AW core properties are calculated based  
429 on each model's AW core depth (details in Section 2c), which varies substantially from model to  
430 model (Heuzé et al. 2022). The models project an increase in AW temperature with a range of 0–7  
431 °C relative to the historical mean towards the end of the 21st century. The AW temperature change  
432 is relatively linear over time and reaches a multi-model mean increase of 3.0 °C in the EB and 2.5  
433 °C in the AB by 2100. Some models predict very weak trends in AW temperature (lowest in the  
434 EB = .013 °C decade<sup>-1</sup>), but the majority predict strong warming (highest in the EB = .740 °C  
435 decade<sup>-1</sup>), in accordance with what was shown by Khosravi et al. (2022). The average future AW  
436 temperature trend in the EB is .33 °C decade<sup>-1</sup>, compared to an observed trend of .06 °C decade<sup>-1</sup>  
437 from 1970–2017. Less intuitive, perhaps, is the future change of AW salinity. Most models  
438 simulate a freshening of the AW layer throughout the Arctic (Table 2), except EC-Earth3 which  
439 simulates an increase in AW salinity in all regions. Averaged across the regions, the multi-model  
440 mean freshening is approximately 0.5 psu by the end of the century, as also shown by Khosravi  
441 et al. (2022).

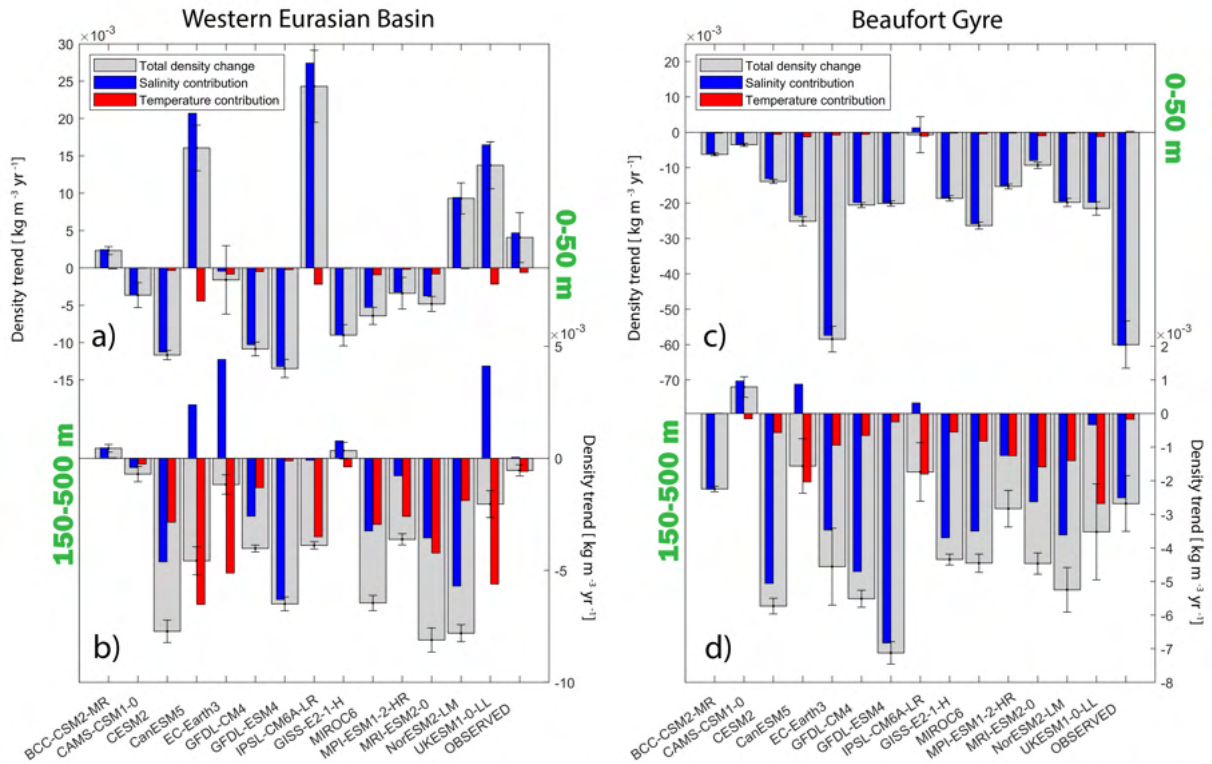
448 The decrease in AW salinity indicates that the northward freshwater flux through the Fram Strait  
449 and Barents Sea Opening increases, which is consistent with results from Zanowski et al. (2021).  
450 Over 2015–2070 all models, except CAMS-CSM1-0 and GFDL-CM4, show a positive trend in the  
451 liquid freshwater flux through the Barents Sea opening, which mainly consists of northward-flowing  
452 AW (Fig. A4b). The freshwater flux through Fram Strait is more complex, as it consists of both a  
453 southward and a northward flow. Here we observe a negative trend in the (northward) freshwater  
454 flux (Fig. A4a), meaning an increase in the net southward freshwater flux. This makes sense, as  
455 the increase in the outflowing freshwater is larger than the increase in the inflowing freshwater (as  
456 it also includes the other freshwater sources). All in all, a decrease in the northward-flowing AW  
457 contributes to a freshening at intermediate depths and ultimately an increase in the total freshwater  
458 content of the Arctic and the southward export of freshwater, as also shown by Zanowski et al.  
459 (2021). Our findings stress an important point that has not been stated in current literature, namely  
460 that the future freshening of the Arctic Ocean may be attributed to both surface and AW changes.  
461 Since there is a strong decoupling between the upper layer and the rest of the deep Arctic in these



442 FIG. 7. Regional time series of normalized (reduced to anomalies relative to 1970–2014 model mean) Atlantic  
 443 Water core temperature (a) and Atlantic Water core salinity (b) from the CMIP6 models listed in Table 1. Thick  
 444 lines represent the multimodel mean, and envelopes show the minimum and maximum of the model spread per  
 445 time step. For comparison, the AW core anomalies from the observations over the 1970–2017 period are shown  
 446 by black lines. The Atlantic Water core properties are calculated as the properties at the temperature maximum  
 447 below 100 m.

462 models, and the AW properties are strongly related to the AW inflow properties (Heuzé et al. 2022),  
 463 we speculate that the Arctic freshening is partly remotely driven.

469 It is important to remember that it is not only the water mass properties but also the depth and  
 470 thickness of the various layers that can affect changes in stratification. We do not detail biases and  
 471 changes in AW core depth but refer the readers to Heuzé et al. (2022) and Khosravi et al. (2022),



464 FIG. 8. Trends (2015–2070) in density in the upper ocean (a) and (c) and at intermediate depth (b) and (d) for  
 465 the Western Eurasian basin (left) and the Beaufort Gyre region (right) for each of the CMIP6 models listed in  
 466 Table 1. Red and blue bars denote the relative contributions of temperature and salinity trends to the total density  
 467 trends (thick grey bars). Positive values mean increased density, and negative values mean decreased density.  
 468 For comparison, the trends from the observations over the 1970–2017 period are shown in the last column.

472 and note that the effects of these changes are integrated in the  $\Delta PE$  metric. As we continue with  
 473 the temperature and salinity evolution of the surface layer (0–50 m), different model behaviors  
 474 become even more evident (Table A1). In the AB, all models project a freshening and warming  
 475 of the surface layer, consistent with current observations (Tab. A1 and Solomon et al. (2021))  
 476 and the expected continuation of AB freshening (Haine 2020). Averaged across the models, the  
 477 absolute change in surface salinity is expected to reach approximately -1.5 psu by the end of the  
 478 century (Fig. A5). In the EB, on the other hand, many models project a freshening, but some  
 479 project a surface salinification (Fig. A5). Some of the models that project a surface salinification  
 480 are the same that project an AW salinification, but for others, there are opposite trends in the AW  
 481 and surface layers. There is no consistent relationship between the direction of surface trends and

482 trends in the AW layer, and there is also no clear relationship between changes in AW/surface  
483 properties and freshwater/salinity fluxes through the Fram Strait and the Barents Sea (not shown).  
484 The multi-model mean still projects a freshening in both the Eastern and Western EB, although  
485 some models have opposing trends. Figs. 7 and A5 emphasize the importance of the regional  
486 aspect when investigating future Arctic Ocean change, and thus provides further detail than the  
487 basin-wide averages provided by Khosravi et al. (2022). Even though the general change is similar  
488 (AW warming and freshening), the regions are projected to evolve somewhat differently or on  
489 different timescales. For example, the Eastern and Western EB are exposed to different processes  
490 as they have a different seasonal ice cover, which is projected to change differently in the future  
491 (Notz and SIMIP Community 2020). Taking an EB or AB mean, as is common practice in CMIP  
492 studies of the Arctic Ocean, is therefore not ideal since one might lose important information and  
493 average out important regional differences. The different evolution in surface properties evident  
494 from Fig. A5 and Table A1 also stresses the importance of studying models individually and not  
495 as a multi model means. These result give an indication to the origin of biases in stratification,  
496 because differences in salinity and temperature trends result in different contributions to the overall  
497 density profile.

498 Fig. 8 shows the comparison of density changes in the upper ocean (0–50 m, lower per panel)  
499 and at intermediate depth below the halocline (150–500 m, lower panel) for each model in the  
500 Western EB and the Beaufort Gyre regions (The Eastern EB and Chukchi regions are shown in  
501 Fig. A6). Red and blue bars denote the relative contributions of temperature and salinity trends to  
502 the total density trends (fat grey bars), respectively. Note the different scales on the y-axis. In the  
503 upper ocean, the density changes are mainly driven by salinity changes. In contrast, at intermediate  
504 depth, the density changes are more equally attributed to both temperature and salinity. In some  
505 cases, temperature and salinity have opposite effects (EC-Earth3 and UKESM1-0-LL), and the  
506 contribution from warming is slightly larger than the salinification, resulting in an overall decrease  
507 in AW density. In other cases, for example in CAMS-CSM1-0, salinification overpowers the  
508 warming. In general, the upper ocean density trends are much larger than the trends at intermediate  
509 depth. Opposing results in the EB stratification are primarily related to opposite changes in surface  
510 density (Fig. 8a). However, density trends further down in the water column also contribute and  
511 may either enhance or diminish the impact of the surface trend on the overall stratification. For

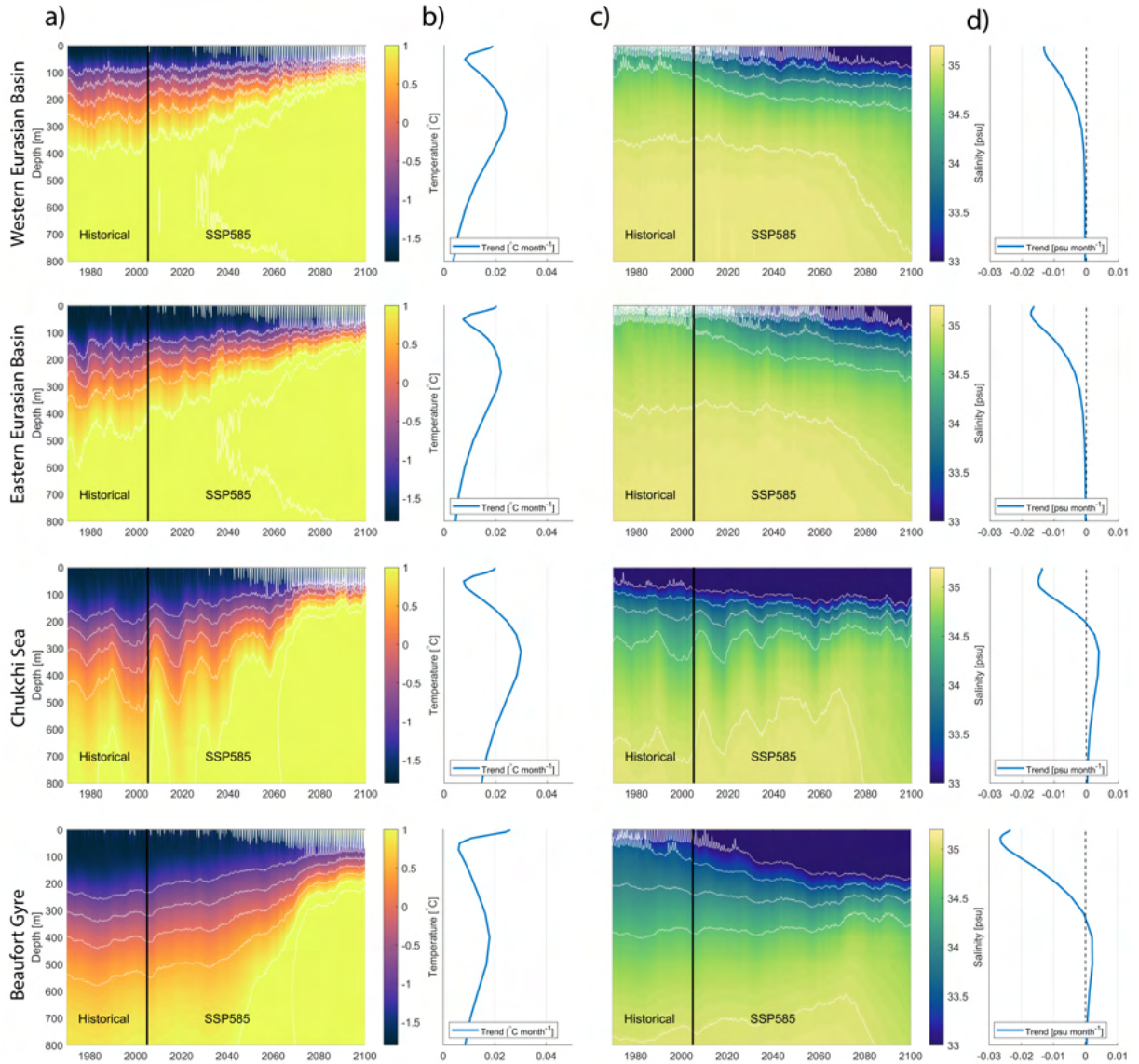


512 example, in the Western EB, changes in the surface and AW layer in CanESM5 contribute to a  
513 weakening of the stratification. In CESM2, on the other hand, the surface trends contribute to  
514 a strengthening of the stratification, and the intermediate layers contribute to a weakening of the  
515 stratification. In summary, the relative change between the upper ocean and intermediate layer  
516 ultimately determines whether the density gradient increases or decreases. We detail these vertical  
517 density gradients and how they change over time in the following section.

#### 518 *d. Future density gradients*

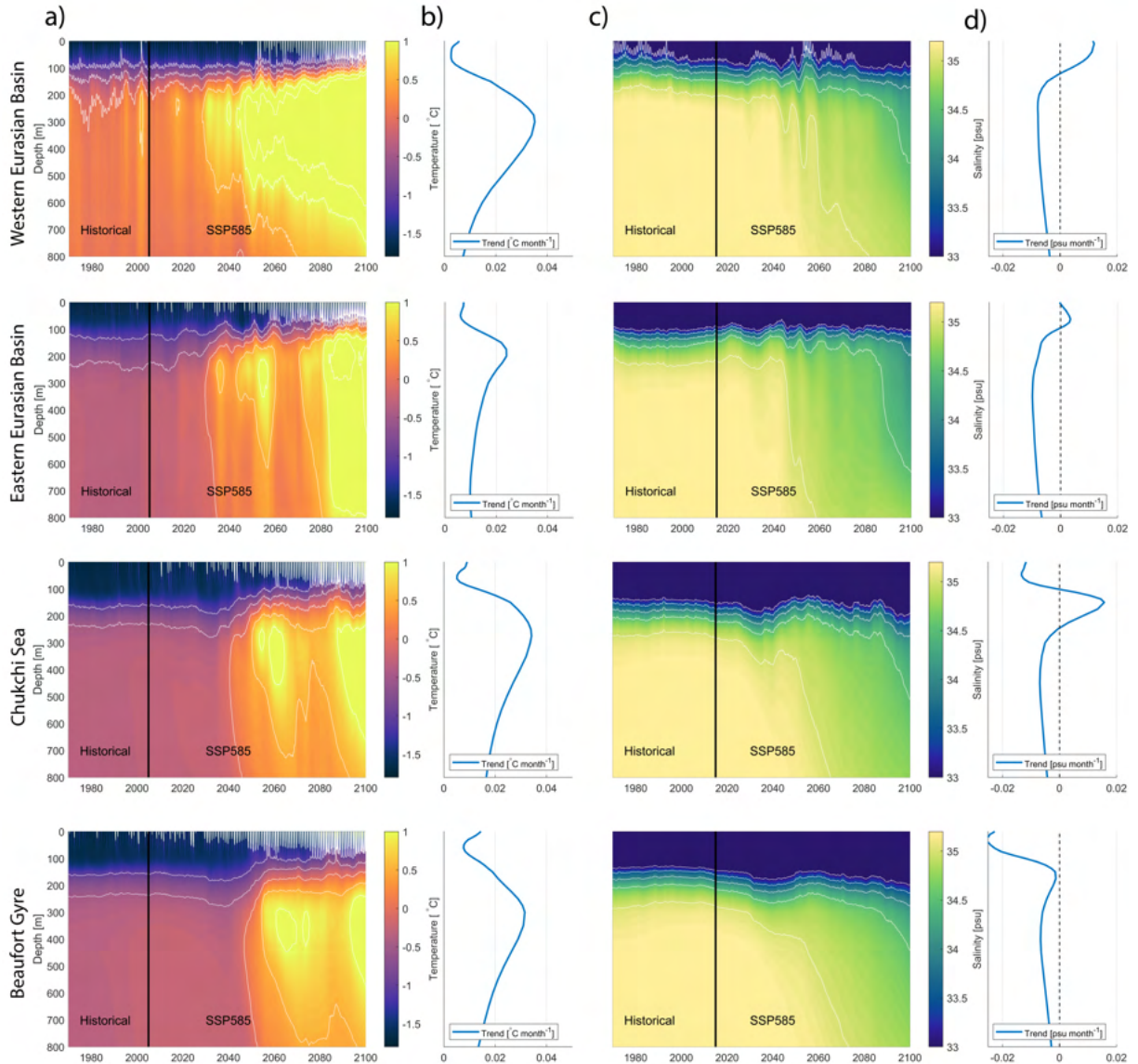
519 We compare two models, GFDL-CM4 and NorESM2-LM, which project distinctly opposite  
520 changes in stratification in the EB (Fig. 6). In Fig. 9 we present the temporal development of  
521 temperature and salinity profiles for the GFDL-CM4 model, which projects a strengthening in  
522 stratification in all regions. Profiles shown in columns b) and d) represent the linear trends in  
523 temperature and salinity at each depth level over 2015–2070. The temperatures are projected to  
524 increase throughout the whole water column, but the change is largest between 200–500 m and  
525 smallest in the halocline, just below the surface mixed layer. These trend profiles might not solely  
526 be due to a change in properties at the given depths but are also a result of the upward or downward  
527 movement of the AW and/or a deepening or shoaling of the SML. Due to space limitations, we  
528 do not investigate these changes in this paper, but Khosravi et al. (2022) give a good overview of  
529 changes in AW core depth and changes in SML depth.

536 The salinity trend profiles (Fig. 9d) show the largest trends at the surface, which gradually  
537 decreases with depth. In this model, below 300 m, there is almost no change in salinity, despite a  
538 small positive trend in AW salinity in the AB regions. This is thus an example of a model where  
539 upper ocean salinity changes primarily drive the stratification changes. These projections appear  
540 plausible, and we can relate the changes to known mechanisms. However, this is a good example  
541 of why it is dangerous to conclude future Arctic Ocean changes based on a single model system:  
542 A study based on a different model system may provide an opposite result. Fig. 10 shows the  
543 temperature and salinity trend profiles for NorESM2-LM, a model which shows a weakening of  
544 the stratification in the EB and a strengthening of stratification in the AB. Overall, the vertical  
545 distribution of temperature trends looks very similar between NorESM2-LM and GFDL-CM4,  
546 which is true for all other models (not shown). Although the absolute values (and mean states) vary



530 FIG. 9. Monthly mean upper ocean temperature (a) and salinity (c) from GFDL-CM4 from 1970 to 2100  
 531 for each region identified in Fig. 1. Linear trends are calculated for each depth level from 2015 to 2070 for  
 532 temperature (b) and salinity (d).

547 from model to model, they all simulate a positive temperature trend throughout the whole water  
 548 column, with a maximum around 200 m depth and a minimum just below the SML. However, the  
 549 salinity trends are very different. In NorESM2-LM (and several other models), there are significant  
 550 salinity trends throughout the whole water column. In NorESM2-LM, the AW salinity decreases  
 551 in all regions, especially after 2040, contributing to the weakening of the stratification. In the AB



533 FIG. 10. Monthly mean upper ocean temperature (a) and salinity (c) from NorESM2-LM from 1970 to 2100  
 534 for each region identified in Fig. 1. Linear trends are calculated for each depth level from 2015 to 2070 for  
 535 temperature (b) and salinity (d).

532 regions, this is balanced by a stronger freshening of the surface, but in the western EB, the surface  
 533 is getting saltier, meaning that both the AW layer and the surface layer contribute to a weakening  
 534 of the density gradient. Fig. 11 shows the trend in density at each depth level over 2015–2070  
 535 for the two models. The combined effects of trend of temperature and salinity yield an overall decrease in  
 536 density throughout the whole upper 800 m of the water column for these two models. In GFDL-

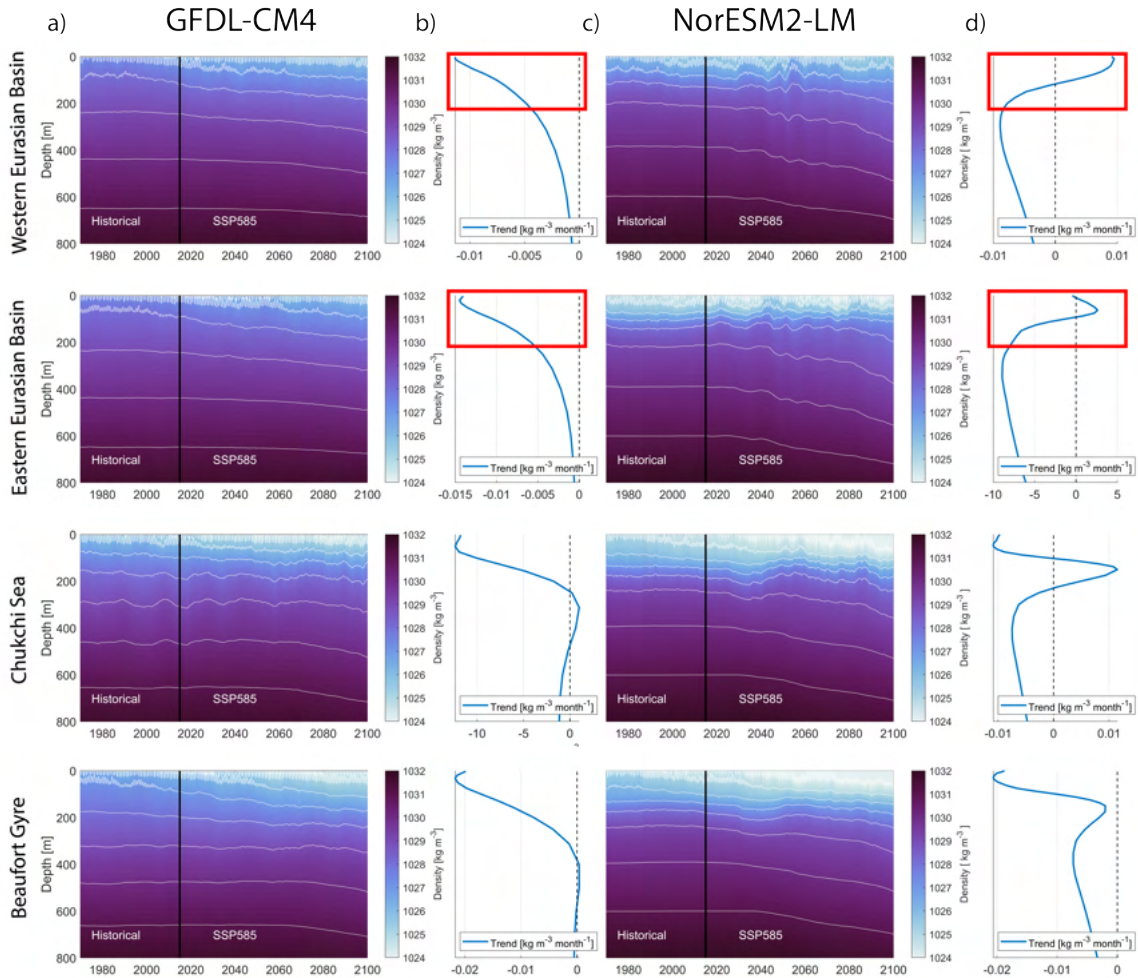
557 CM4, the profiles look similar for all four regions, with the largest decrease in the upper ocean and  
558 gradually decreasing trends with depth, increasing the gradient between the upper and intermediate  
559 layers. In NorESM2-LM, the profiles in the AB look similar, but in the EB regions, the (negative)  
560 density trend increases with depth in the upper 200 m (red box, Fig. 11), resulting in a decreased  
561 density gradient there. The density trend profiles provide a nice way to compare the hydrographic  
562 changes with depth in the various regions and highlight how differently the hydrographic structure  
563 is transformed in the multiple models under a similar climatic forcing. The density trend profiles  
564 for all models are shown in Fig. 12.

570 In the EB, most models agree on a negative density trend below 200 m, but above they diverge.  
571 Here we also see large discrepancies in how quickly the density trends increase or decrease with  
572 depth, thus the extent of the water column that is changed. Again, this is related to the SML depth,  
573 which varies and changes differently over time (Fig. 12). In the Beaufort Gyre region, the models  
574 have a very similar shape, but already in the Chukchi Sea, we see that models start to diverge, with  
575 some projecting densification of the water column and some projecting a negative trend in density  
576 throughout the water column. To summarize, there are many reasons why the models diverge on  
577 future stratification in the EB – the divergence is partly related due to different/opposite trends  
578 at the surface and partly due to a different balance between the strength of density trends at the  
579 surface and at AW depth, or both.

#### 584 *e. Atlantification in the future*

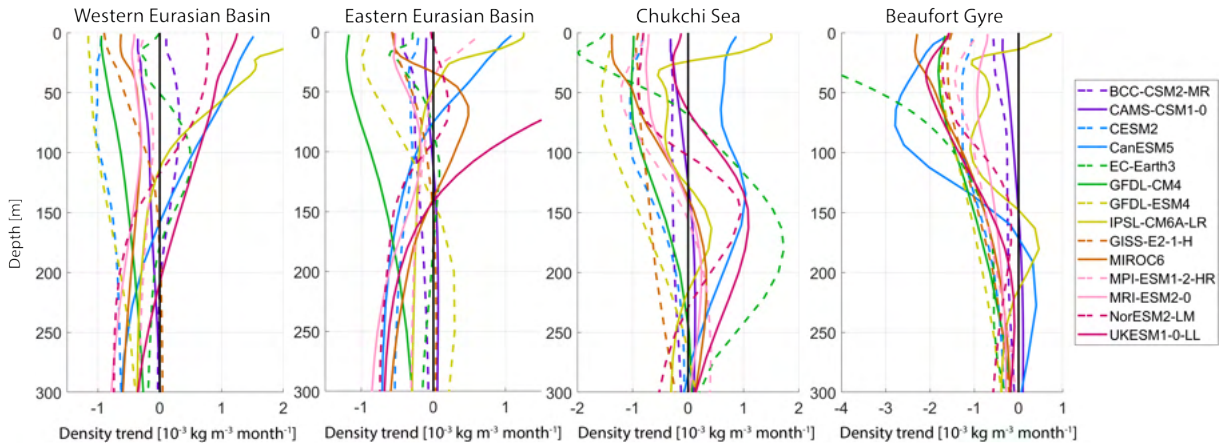
585 Under the ssp585 strong greenhouse-gas forcing scenario, there is good agreement among the  
586 models that the Arctic Ocean will continue to warm into the future with the largest warming in the  
587 AW layer and the EB. Accompanying this warming is a northward shift of ecosystems (Polyakov  
588 et al. 2020a, and references therein), a diminishing sea ice cover (Notz and SIMIP Community  
589 2020), and further changes that we can combine under the term Atlantification, as parts of the  
590 Arctic Ocean gradually become more similar to the North Atlantic. However, it is not given  
591 whether Atlantification will continue to be a metonymy for “weakening in stratification” – its  
592 primary manifestation in the EB in recent decades (Polyakov et al. 2017).

593 The implications of changing stratification are numerous. As highlighted by Polyakov et al.  
594 (2020a), it can affect vertical fluxes of nutrients and dissolved gasses and hence impact biology,



565 FIG. 11. Monthly mean upper ocean density from GFDL-CM4 (a) and NorESM2-LM (c) from 1960 to 2100  
 566 for the regions identified in Fig. 1. Linear trends are calculated for each depth level from 2015 to 2070 for  
 567 GFDL-CM4 (b) and NorESM2-LM (d). Red boxes indicate the depth interval in the Western EB and Eastern EB  
 568 regions where the slope of the density trend profile is opposite for the two models, resulting in opposite changes  
 569 to the stratification.

595 but it mainly affects the vertical distribution of heat and hence the sea ice cover. Khosravi et al.  
 596 (2022) also mention the potential impact of model biases on the simulated sea ice cover. We,  
 597 therefore, investigate whether there is a relationship between the diverging stratification trends and  
 598 the rate of sea ice decline in the EB. We now focus on the trends in the first half of the future  
 599 scenario (2015–2045) where there is still sea ice left in the EB. The top panels of Fig. 13 show



580 FIG. 12. Regional vertical profiles of the linear trend in density (similar to Fig. 11b and 11d) over the period  
 581 2015–2070 from the CMIP6 models listed in Table 1. A stronger (negative) trend near the surface (~0–100 m)  
 582 compared to intermediate depths (~150–300 m) results in a strengthened stratification. Note the different x-axis  
 583 for each panel.

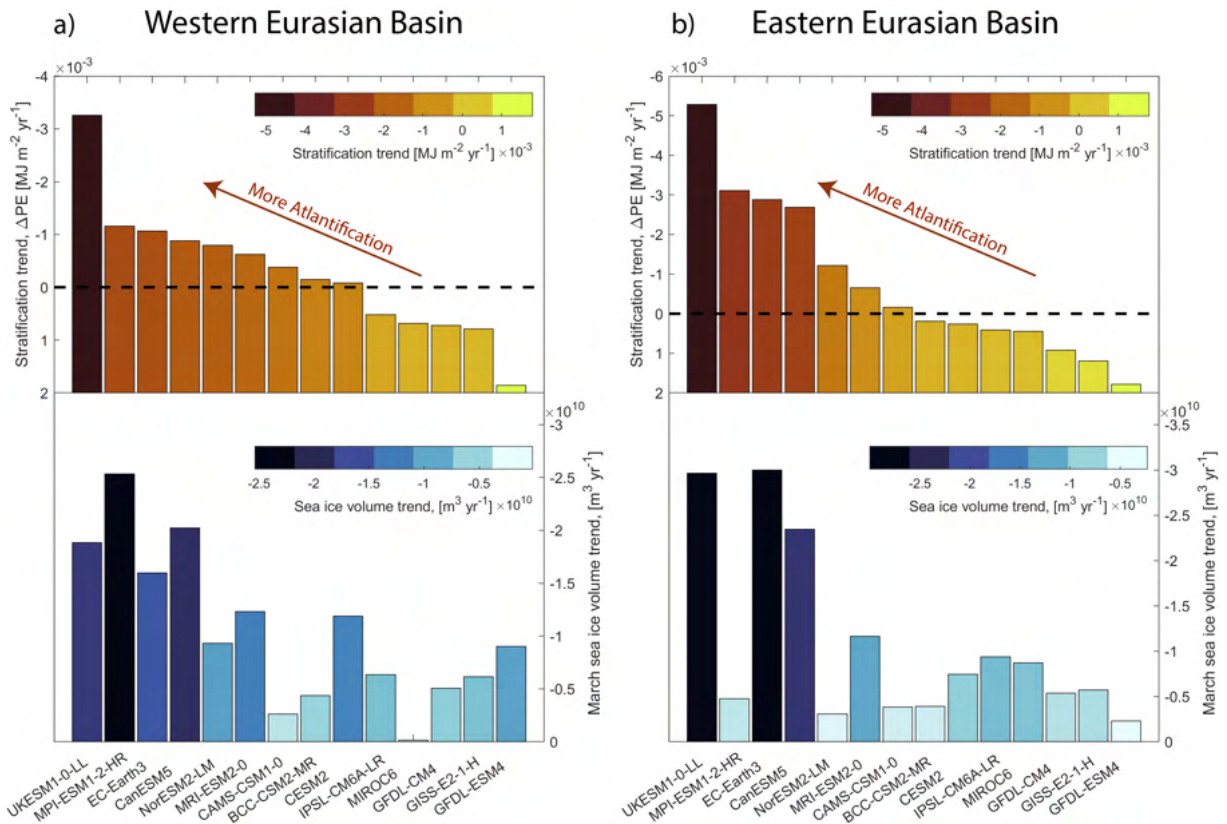
600 the future “degree” of Atlantification (here arranged in order of decreasing stratification trend)  
 601 for the different models in the EB. Models projecting the strongest weakening of stratification are  
 602 found towards the left and those projecting the strongest increase in stratification are found towards  
 603 the right. Similarly to Fig 6, CanESM5, UKESM1-0-LL, EC-Earth3 and MPI-ESM1-2-HR are  
 604 the models with the strongest degree of future Atlantification in both the Western and Eastern  
 605 EB. IPSL-CM6A-LR also shows strong Atlantification in the Western EB and NorESM2-LM also  
 606 shows strong Atlantification in the Eastern EB. In contrast, GFDL-CM4, GFDL-ESM4 and GISS-  
 607 E2-1-H have the smallest degree of future Atlantification as they project an increase in stratification  
 608 in both regions. The lower panels in Fig. 13 show the trends in winter (March) sea ice volume  
 609 in these regions following the same order as the panels above. From these figures we see that the  
 610 models with strongest degree of Atlantification, i.e. weakened stratification, project the strongest  
 611 decline in sea ice in these parts of the EB. This is not surprising; although there are many factors  
 612 influencing the sea ice trend, the ocean plays an increasingly important role, especially in the EB  
 613 (Carmack et al. 2015). Our results show an across-model correlation of  $r = 0.64$  between the sea  
 614 ice volume trends and stratification trends in the Western EB and an across-model correlation of  
 615  $r = 0.76$  in the Eastern EB (statistically significant at 95% level). The relationship is not perfect  
 616 and this is likely related to the mean sea ice state of the models or other important processes.

617 For example, MPI-ESM1-2-HR has a very weak decline in sea ice volume compared to its strong  
618 degree of Atlantification in the Eastern EB, but since it finished the historical run with a low sea ice  
619 thickness compared to the other models (not shown), it simply cannot have a large volume trend.  
620 For reference we have therefore provided a table of mean sea ice volume at the beginning and in the  
621 middle of the ssp585 scenario (Table A2). Although correlation does not imply causation, there  
622 appears to be some relationship or commonality among the models that have a faster decline of sea  
623 ice and a weakening of stratification in the EB.

624 Since the models are roughly equally divided among two different stratification scenarios, it  
625 is unclear whether the currently ongoing weakening of the stratification in the EB will continue  
626 or not. Following Heuzé et al. (2022) and Khosravi et al. (2022), there is no clear evidence of  
627 certain models being significantly better at accurately reproducing the Arctic Ocean hydrography  
628 and circulation, and we can therefore not favor certain models or either of the scenarios. There  
629 is also no clear relationship between models with higher or lower resolution. As suggested by  
630 our companion paper, Heuzé et al. (2022), improvements could focus on ventilation, dense water  
631 overflows and inflow properties. There are also large biases in AW flow speed and patterns, and  
632 most CMIP6 models show a strong decoupling between the upper layers and the rest of the deep  
633 Arctic not consistent with observations.

#### 639 **4. Discussion and conclusions**

640 This study quantified recent and future trends in upper Arctic Ocean stratification, temperature,  
641 and salinity in an ensemble of 14 CMIP6 models and compared these to a unique dataset of  
642 hydrographic observations dating back to 1970. In agreement with observations (e.g. Polyakov  
643 et al. 2020a), the models simulate a freshening and warming of the upper Amerasian basin (AB) and  
644 large parts of the Eurasian Basin (EB) over the period 1970–2014. These changes are associated  
645 with a general strengthening of the stratification, but there is a large spread among the simulated  
646 trends and mean stratifications. Although only three out of the 14 models simulate a weakening of  
647 the stratification in the EB that is comparable to observations, all models indicate different trends  
648 in stratification in the AB and EB. We note that for the 1970–2014 period, forcing is modest and  
649 internal variability likely influences these trends.



634 FIG. 13. Top panels: "Degree" of future Atlantification in the Western (a) and Eastern (b) Eurasian basin,  
 635 defined by trends in  $\Delta P E$  (2015–2045). The models are arranged in order of decreasing stratification trend, with  
 636 models projecting the strongest weakening of stratification towards the left and strongest increase in stratification  
 637 towards the right. Lower panels: Trends in winter (March) sea ice volume (2015–2045) for each of the models,  
 638 following the same order as the panels above. The length of the bars and their colours indicate the same values.

650 Because of temperature, salinity, and stratification biases in CMIP models, simulating and defin-  
 651 ing the halocline in models is challenging, especially when studying it in a suite of models under  
 652 a climate change scenario. To compare and evaluate simulated Arctic stratification meaningfully,  
 653 we, therefore, proposed a new indicator of stratification,  $\Delta P E$ . This is an integral of the potential  
 654 energy needed to fully mix the water column from the surface down to 300 m depth. Typical Arctic  
 655 Ocean values are about  $0.1 \text{ MJ m}^{-2}$ , but the Beaufort Gyre and the Chukchi Sea have twice as strong  
 656 stratification. Temporal change and regional contrasts observed by more traditional stratification  
 657 definitions (e.g. Polyakov et al. 2020a) are captured well by this new parameter, whose definition  
 658 is not sensitive to model biases.



659 There is a reassuring across-model agreement within the Beaufort Gyre and the Chukchi Sea  
660 for near-surface stratification. Here the upper ocean layer will become fresher (on average 0.18  
661 psu decade<sup>-1</sup>), warmer (on average 0.35 °C decade<sup>-1</sup>) and more stratified in the future (on average  
662  $1.1 \times 10^{-4}$  MJ m<sup>-2</sup> decade<sup>-1</sup>), but there is a large spread in the magnitude (likely due to different  
663 freshwater input and differences in the freshwater pathways). There is also simulated future  
664 warming (0.24 °C decade<sup>-1</sup>) and freshening (-0.03 psu decade<sup>-1</sup>) occurring further down in the  
665 Atlantic Water (AW) layer. The entire water column is therefore getting less dense, but the  
666 surface freshening is so strong that the stratification is overall increasing in these regions. We  
667 did not examine the detailed causes of the future surface freshening but hold it as likely that  
668 both redistribution and local melting of sea ice, increased river runoff, increased glacial melt, and  
669 increased freshwater inflow through Bering Strait will all contribute significantly – as they do today  
670 (Haine et al. 2015; Haine 2020; Solomon et al. 2021). Throughout the upper Arctic Ocean, density  
671 trends are dominated by changes in salinity, but at intermediate depth, temperature and salinity  
672 changes contribute equally to the density trends.

673 In both the Eastern and Western EB, there is a divergence between the models regarding future  
674 stratification. Approximately half of the models project a strengthening of stratification here,  
675 and the other half project the opposite. The divergence is partly caused by opposing trends in  
676 upper ocean temperature and salinity. Additionally, the divergence is related to different spatial  
677 extent of the Atlantification and Pacification signals, not captured in the analysis due to the use of  
678 fixed regions. Furthermore, we discuss how the differences in stratification are related to different  
679 balances between trends in the upper ocean and trends at intermediate depths. Across the suite of  
680 models, there is a warming of the EB AW layer, but it varies between 0-7°C towards the end of  
681 the century. A majority of the models also project a freshening of the EB AW layer (0-0.9 psu),  
682 starting approximately in the 2050s. The AW warming and freshening result in a reduced density  
683 at intermediate depths, weakening the stratification. In about half of the models, these changes  
684 are counterbalanced by an upper-ocean freshening resulting in a strengthened stratification also in  
685 the EB. However, in some models, parts of the EB upper ocean experience a salinification, or the  
686 AW density change dominates (or both), aiding to an overall weakened stratification. It is difficult  
687 to judge which of the two stratification scenarios is the most likely. The divergence appears to  
688 impact the projections of sea ice, and we report on an across-model correlations ( $r = 0.64$  and

689  $r = 0.76$ ) between the trends in sea ice volume and trends in stratification. The models that project  
690 a weakened stratification in the EB also project a stronger decline in sea ice volume here.

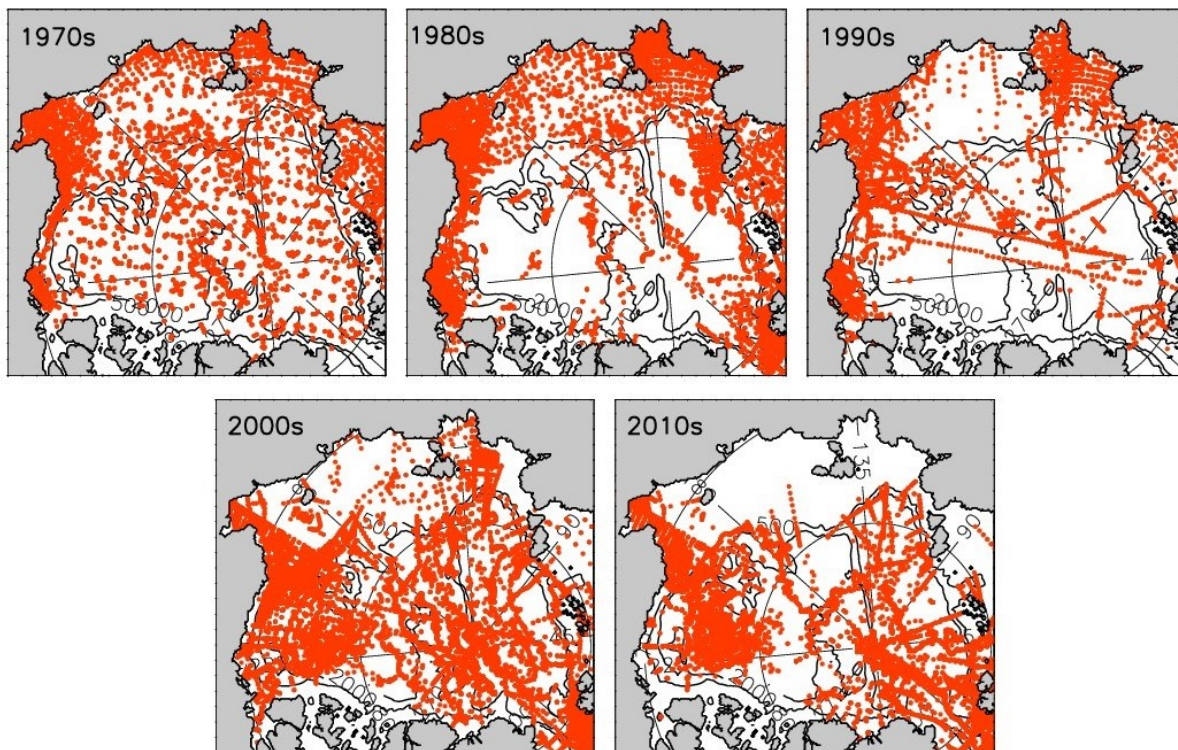
691 In summary, observations and simulations agree that the Arctic Ocean is becoming warmer and  
692 that there is ongoing freshening in the AB. The simulations also agree that the observed weakening  
693 of the stratification in the EB does not spread eastward into the AB. The warming is unsurprising  
694 on a globally warming planet, and the future warming of the AW layer is most pronounced. In that  
695 regard, it is consistent with using the term Atlantification – as these waters are becoming more  
696 similar to those further south. However, it is unclear whether Atlantification will continue to be  
697 analogous to a weakening in stratification. Of the models we analyzed, half of the models predicted  
698 a strengthening of the EB stratification. This is not what is currently associated with Atlantification.  
699 Further work is thus required before we can have more confidence in the future development of the  
700 EB. First, we need to improve the model’s capability to simulate Arctic hydrography. Particular  
701 emphasis should be on the representation of AW circulation, ventilation, and the connections  
702 between the shelves and the deep basins (Heuzé et al. 2022). Additionally, there is an urgent need  
703 for more multi-scale (in time and space) observational campaigns, such as the recent MOSAiC  
704 expedition (Rabe et al. 2022), that simultaneously provide in-situ data of all the components of the  
705 Arctic climate system. Such campaigns result in a better understanding of specific processes and  
706 their interaction, which then can be used to improve their representation in the models. Long-term  
707 mooring deployments in the Central Arctic are also needed to understand the variability at various  
708 timescales.

709 Our study highlights the importance of a multi-model approach for studies of the future Arctic  
710 Ocean. Given the relatively large biases and opposite trends, relying on a single or just a few  
711 model systems is insufficient and may result in misleading conclusions. However, it is important to  
712 analyze and interpret the models individually, not as a multi-model mean. Our results clearly show  
713 that averaging (opposite) model trends and properties will yield results that seem credible but are  
714 completely nonphysical. This is particularly important for profiles - as water masses are distributed  
715 differently in the vertical, and the same processes, therefore, have an effect at different depths.  
716 Thus, an important takeaway from this study is that we strongly discourage using multi-model  
717 averages to investigate trends in Arctic hydrography. Also, many ensembles from a single model  
718 system may skew the results towards specific model biases created by physical or thermodynamical

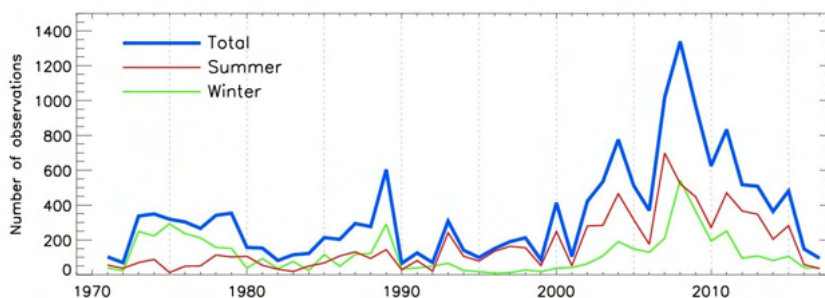
719 deficiencies. However, studies using many ensembles could give important information about the  
720 relative importance of internal variability compared to external forcing, and we stress the need for  
721 such analysis. Clearly, studies of the Arctic Ocean should be based on and validated by observations  
722 due to the inherent large local uncertainty of the models.

723 *Acknowledgments.* Morven Muilwijk received funding for this work from the European Union's  
724 Horizon 2020 research and innovation programme under grant agreement No 101003826 via  
725 project CRiceS (Climate Relevant interactions and feedbacks: the key role of sea ice and Snow  
726 in the polar and global climate system) and from the University of Bergen, Bjerknes Center for  
727 Climate Research. Aleksi Nummelin received funding for this work from Research Council of  
728 Norway project KeyClim (295046). Igor V. Polyakov acknowledges support from the United States  
729 NSF grants (AON-1724523, AON-1947162) and ONR grant (N00014-21-1-2577). Céline Heuzé  
730 received funding for this work from Vetenskapsrådet under grant agreement 2018-03859. Support  
731 for Hannah Zanowski was provided by the Office of the Vice Chancellor for Research and Graduate  
732 Education at the University of Wisconsin–Madison with funding from the Wisconsin Alumni  
733 Research Foundation. Lars H. Smedsrud was supported by the Norwegian Research Council  
734 through the Nansen Legacy Project (Grant#276730). The authors acknowledge the World Climate  
735 Research Programme, which, through its Working Group on Coupled Modelling, coordinated and  
736 promoted CMIP6. The authors also thank the various modeling groups for producing and making  
737 their model output available, the Earth Grid System Federation (ESGF) for archiving and providing  
738 access, and the multiple funding agencies that support CMIP6 and ESGF. Computing and storage  
739 resources were provided by Sigma2 - the National Infrastructure for High-Performance Computing  
740 and Data Storage in Norway, and the authors would like to thank Michael Schulz, Yanchun He,  
741 and Richard Davy for coordinating the local storage of CMIP6 data and Anais Bretones for support  
742 with the data download. The authors would also like to thank those who went to sea and collected  
743 valuable observations in harsh Arctic conditions over the last century. Finally, we thank the three  
744 anonymous reviewers, as well as the editor Laure Zana, for their many comments that greatly  
745 improved this manuscript.

746 *Data availability statement.* CMIP6 data are freely available via the Earth Grid System Federation.  
747 For the analysis presented here, we used the Geophysical Fluid Dynamics Laboratory (GFDL) node:  
748 <https://esgdata.gfdl.noaa.gov/search/cmip6-gfdl/> and the Lawrence Livermore Na-  
749 tional Laboratory node: <https://esgf-node.llnl.gov/projects/cmip6/>. Annual mean  
750 temperature and salinity profiles over the historical period (1970–2017) from the observations and  
751 CMIP6 models used in this study are available from ? at [doi provided upon acceptance].

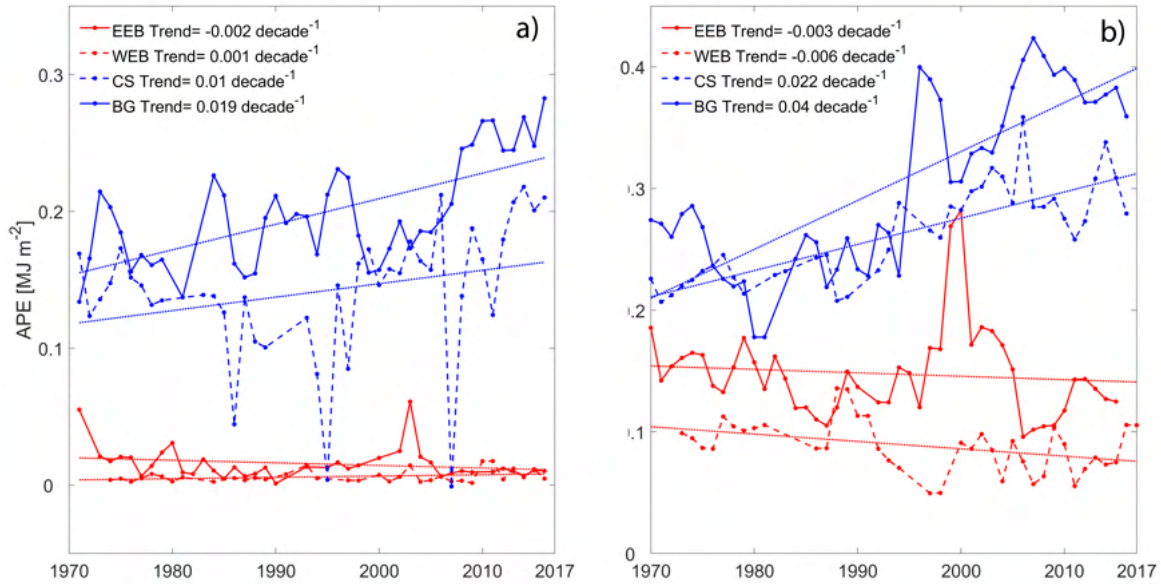


753 FIG. A1. Temporal and spatial data coverage for each of the decades in the observational data set used in this  
 754 study. Annual mean profiles are available through the Arctic Data Center (?).

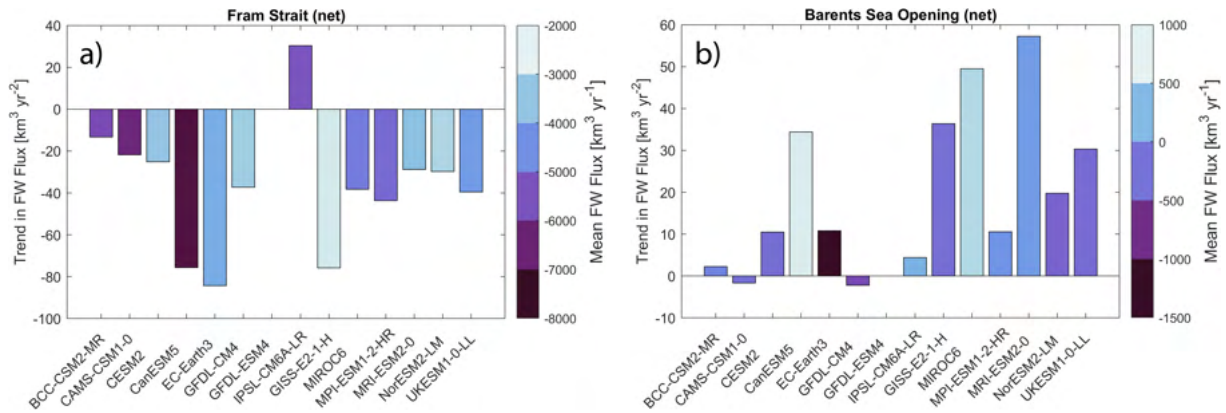


755 FIG. A2. Number of hydrographic observations per season for the Eurasian basin and Amerasian basin regions  
 756 combined.

752 APPENDIX



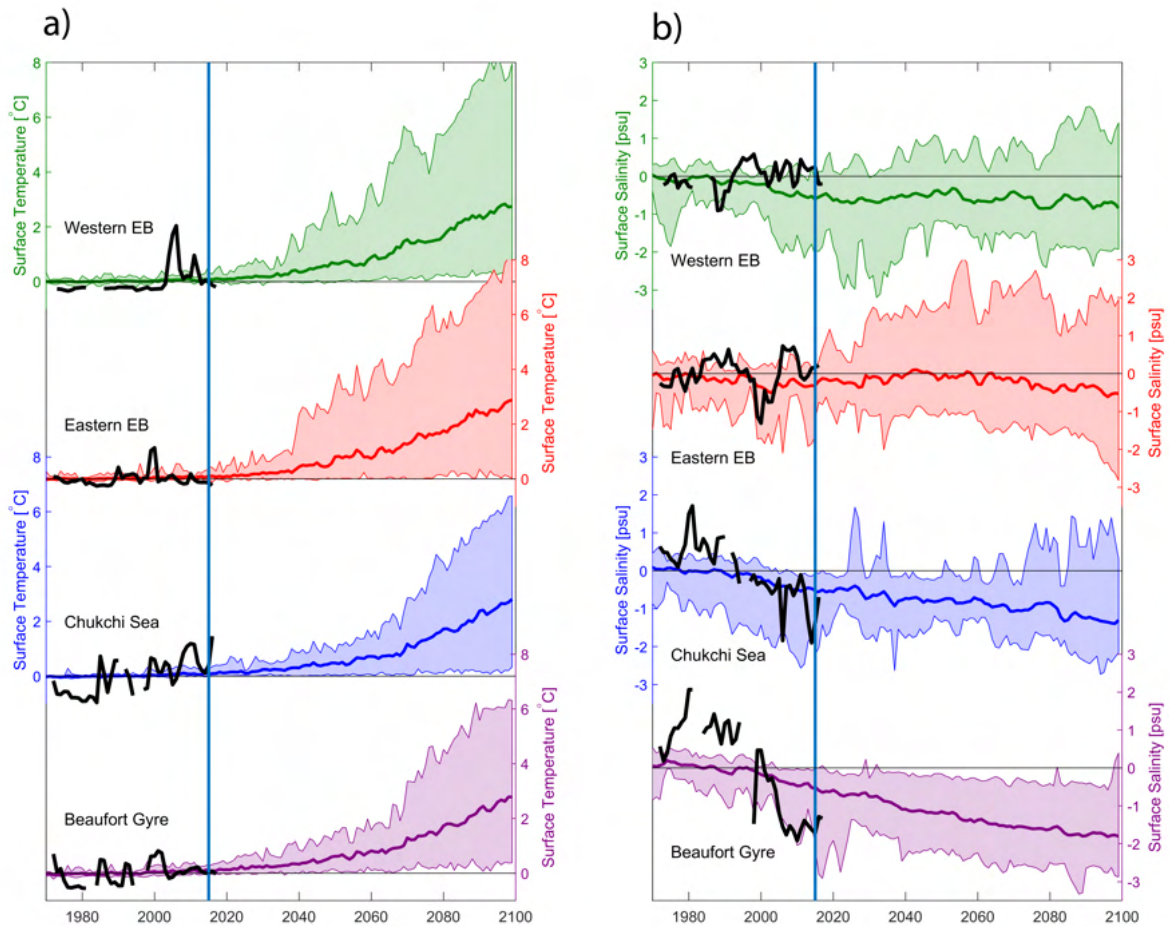
757 FIG. A3. Observed annual mean stratification within the Arctic Ocean using two different measures. a)  
 758 available potential energy (APE) following equation (2), and b) potential energy stored in stratification ( $\Delta PE$ )  
 759 from 300 m following equation (4). Blue colors are used for the AB, and red colors are used for EB. WEB  
 760 = Western Eurasian basin, EEB = Eastern Eurasian basin, CS = Chukchi Sea and BG = Beaufort Gyre. In a)  
 761 only the BG trend is statistically significant ( $p \geq 0.05$ ), whereas in b) all trends, except the EEB, are statistically  
 762 significant. By definition, APE is directly linked to halocline base depth and is, therefore, an order of magnitude  
 763 larger in the AB than in the EB.



764 FIG. A4. Trends in net liquid freshwater flux ( $\text{km}^3 \text{yr}^{-2}$ ) from 2015–2020 at a) Fram Strait and b) the Barents  
 765 Sea Opening for the ssp585 future scenario. Color shading indicates the mean net liquid freshwater flux for each  
 766 model over the same time period. Positive direction is northward (Fram Strait experiences a net southward flux  
 767 of freshwater). Velocity data from GFDL-ESM4 was not available and therefore no fluxes could be calculated  
 768 for this model.

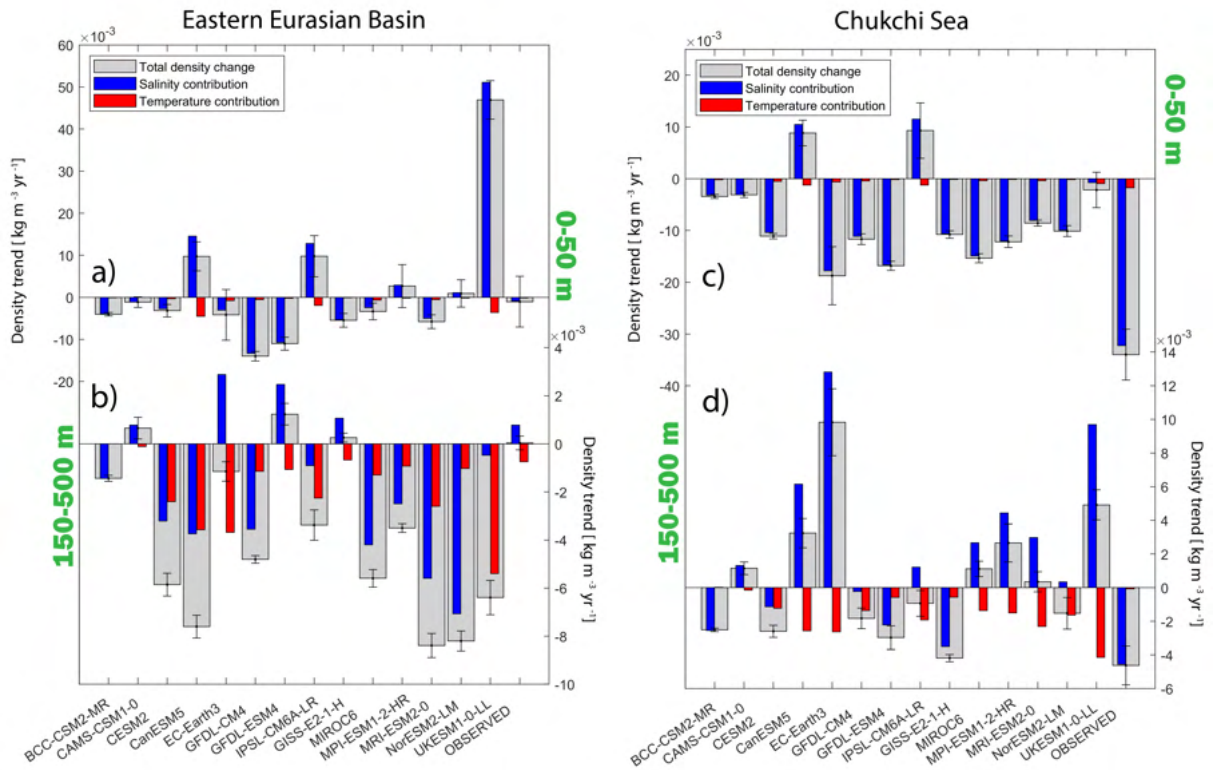
779 TABLE A1. Future upper ocean (0–50 m) temperature and salinity trends for each of the CMIP6 models  
 780 (forcing scenario ssp585) over 2015–2020. For comparison, the last row indicates the trends for the observations  
 781 over the 1970–2017 period. All values are given in  $^{\circ}\text{C} \text{decade}^{-1}$  and  $\text{psu} \text{decade}^{-1}$ . Statistically non-significant  
 782 trends ( $p \geq 0.05$ ) are shown in italic.

	Western EB		Eastern EB		Chukchi Sea		Beaufort Gyre	
	$\theta$	$S$	$\theta$	$S$	$\theta$	$S$	$\theta$	$S$
BCC-CSM2-MR	.044 ± .006	.030 ± .007	.049 ± .007	-.048 ± .005	.083 ± .011	-.039 ± .005	.082 ± .017	-.074 ± .005
CAMS-CSM1-0	.018 ± .004	-.045 ± .021	.006 ± .003	-.014 ± .016	.012 ± .003	-.038 ± .006	.023 ± .008	-.043 ± .005
CESM2	.124 ± .009	-.139 ± .007	.134 ± .014	-.034 ± .019	.183 ± .017	-.129 ± .007	.189 ± .017	-.163 ± .007
CanESM5	.823 ± .044	.252 ± .037	.857 ± .039	.172 ± .042	.374 ± .018	.125 ± .031	.381 ± .019	-.307 ± .016
EC-Earth3	.191 ± .021	-.021 ± .053	.166 ± .022	-.052 ± .067	.176 ± .022	-.227 ± .069	.258 ± .013	-.703 ± .047
GFDL-CM4	.138 ± .012	-.127 ± .011	.150 ± .015	-.167 ± .014	.153 ± .013	-.139 ± .013	.175 ± .016	-.252 ± .009
GFDL-ESM4	.067 ± .009	-.163 ± .015	.087 ± .012	-.136 ± .018	.070 ± .008	-.209 ± .011	.077 ± .009	-.251 ± .009
IPSL-CM6A-LR	.393 ± .035	.279 ± .053	.299 ± .029	.099 ± .051	.258 ± .021	.060 ± .071	.238 ± .022	-.064 ± .066
GISS-E2-1-H	.022 ± .003	-.106 ± .017	.043 ± .004	-.063 ± .019	.061 ± .008	-.132 ± .009	.081 ± .007	-.232 ± .009
MIROC6	.271 ± .027	-.064 ± .015	.209 ± .023	-.022 ± .025	.133 ± .012	-.182 ± .011	.131 ± .016	-.319 ± .012
MPI-ESM1-2-HR	.071 ± .009	-.040 ± .026	.083 ± .009	.036 ± .063	.061 ± .008	-.149 ± .014	.093 ± .011	-.186 ± .009
MRI-ESM2-0	.197 ± .020	-.049 ± .013	.148 ± .023	-.062 ± .020	.104 ± .020	-.102 ± .007	.230 ± .022	-.110 ± .010
NorESM2-LM	.032 ± .006	.116 ± .026	.066 ± .009	.017 ± .040	.071 ± .009	-.125 ± .013	.103 ± .012	-.246 ± .014
UKESM1-0-LL	.491 ± .030	.190 ± .039	.714 ± .056	.583 ± .054	.272 ± .014	-.019 ± .043	.320 ± .017	-.269 ± .024
OBSERVED	.174 ± .058	.093 ± .038	.018 ± .032	.041 ± .052	.355 ± .054	-.451 ± .056	.086 ± .043	-.745 ± .078



769 FIG. A5. Regional time series of normalized (reduced to anomalies relative to 1970-2014 model mean) upper  
 770 ocean temperature (a) and upper ocean salinity (b) from the CMIP6 models listed in Table 1. Thick lines represent  
 771 the multimodel mean and envelopes shows the minimum and maximum of the model spread per time-step. For  
 772 comparison, the AW core anomalies from the observations over the 1970–2017 period are shown by black lines.  
 773 The upper ocean properties are calculated as the vertical average between 0–50 m.





774 FIG. A6. Trends in density in the upper ocean (a) and c)) and Atlantic Water layer (b) and d) for the Eastern  
 775 Eurasian basin (left) and the Chukchi Sea region (right) for each of the CMIP6 models listed in Table 1. Red and  
 776 blue bars denote the relative contributions of temperature and salinity trends to the total density trends (fat grey  
 777 bars). Positive values mean increased density and negative values mean decreased density. For comparison, the  
 778 trends from the observations over the 1970–2017 period are shown in the last column.

783 TABLE A2. Mean values of winter (March) sea ice volume for each of the CMIP6 models at the beginning  
 784 (2015–2020) and in the middle (2045–2050) of the future scenario (ssp585). Values are given in  $\times 10^{12} m^3$ .

	Western EB		Eastern EB		Chukchi Sea		Beaufort Gyre	
	2015–2020	2045–2050	2015–2020	2045–2050	2015–2020	2045–2050	2015–2020	2045–2050
BCC-CSM2-MR	0.7048	0.4337	0.8561	0.6712	1.1655	0.7692	1.2434	0.8215
CAMS-CSM1-0	0.8055	0.6962	1.3052	1.0304	2.0040	1.3589	1.7776	1.3248
CESM2	0.7830	0.3929	0.8625	0.5532	1.2570	0.5941	1.4175	0.7436
CanESM5	0.6003	0.0609	0.9030	0.1920	1.7197	0.3736	1.9832	0.5563
EC-Earth3	0.9706	0.4577	1.5048	0.6637	2.5761	0.9336	2.7081	1.0866
GFDL-CM4	0.6613	0.3053	0.8851	0.6476	1.7695	1.0893	1.8723	1.0438
GFDL-ESM4	0.6876	0.4621	0.9285	0.7643	1.8496	1.2876	1.7012	1.2128
IPSL-CM6A-LR	2.1841	1.5524	1.1954	0.9114	1.7503	1.2596	1.7637	1.2277
GISS-E2-1-H	0.5985	0.3249	0.8767	0.5319	1.5529	0.8210	1.9020	0.9901
MIROC6	0.9845	0.3676	1.0751	0.5134	2.1653	0.9727	2.2407	1.2120
MPI-ESM1-2-HR	0.7722	0.5795	1.0548	0.8749	1.5991	1.2210	1.8286	1.1798
MRI-ESM2-0	0.4743	0.2265	0.8716	0.6045	1.2926	0.7827	1.4354	0.7448
NorESM2-LM	0.8201	0.5879	0.9580	0.7057	1.6360	1.0659	1.8859	1.0683
UKESM1-0-LL	1.1630	0.2188	1.5363	0.3350	2.7731	0.7954	2.8335	0.9156

## 785 **References**

- 786 Aagaard, K., L. Coachman, and E. Carmack, 1981: On the halocline of the Arctic Ocean. *Deep*  
787 *Sea Research Part A. Oceanographic Research Papers*, **28 (6)**, 529–545, [https://doi.org/10.1016/](https://doi.org/10.1016/0198-0149(81)90115-1)  
788 0198-0149(81)90115-1.
- 789 Adcroft, A., and Coauthors, 2019: The GFDL global ocean and sea ice model OM4. 0: Model  
790 description and simulation features. *Journal of Advances in Modeling Earth Systems*, **11 (10)**,  
791 3167–3211, <https://doi.org/10.1029/2019MS001726>.
- 792 Amante, C., and B. W. Eakins, 2009: ETOPO1 Global Relief Model converted to PanMap layer  
793 format. *NOAA-National Geophysical Data Center, PANGAEA*.
- 794 Årthun, M., and T. Eldevik, 2016: On anomalous ocean heat transport toward the Arctic and  
795 associated climate predictability. *Journal of Climate*, **29 (2)**, 689–704, [https://doi.org/10.1175/](https://doi.org/10.1175/JCLI-D-15-0448.1)  
796 JCLI-D-15-0448.1.
- 797 Årthun, M., T. Eldevik, L. H. Smedsrud, O. Skagseth, and R. B. Ingvaldsen, 2012: Quantifying  
798 the Influence of Atlantic Heat on Barents Sea Ice Variability and Retreat. *Journal of Climate*,  
799 **25 (13)**, 4736–4743, <https://doi.org/10.1175/JCLI-D-11-00466.1>.
- 800 Bluhm, B., K. Kosobokova, and E. Carmack, 2015: A tale of two basins: An integrated physical  
801 and biological perspective of the deep Arctic Ocean. *Progress in Oceanography*, **139**, 89–121,  
802 <https://doi.org/10.1016/j.pocean.2015.07.011>.
- 803 Bluhm, B. A., and Coauthors, 2020: The Pan-Arctic Continental Slope: Sharp Gradients of  
804 Physical Processes Affect Pelagic and Benthic Ecosystems. *Frontiers in Marine Science*, **7**,  
805 544–586, <https://doi.org/10.3389/fmars.2020.544386>.
- 806 Bourgain, P., and J. Gascard, 2011: The Arctic Ocean halocline and its interannual variability from  
807 1997 to 2008. *Deep Sea Research Part I: Oceanographic Research Papers*, **58 (7)**, 745–756,  
808 <https://doi.org/10.1016/j.dsr.2011.05.001>.
- 809 Carmack, E., and Coauthors, 2015: Towards Quantifying the Increasing Role of Oceanic Heat  
810 in Sea Ice Loss in the New Arctic. *Bulletin of the American Meteorological Society*, **96 (12)**,  
811 2079–2105, <https://doi.org/10.1175/BAMS-D-13-00177.1>.

- 812 Carmack, E. C., 2007: The alpha/beta ocean distinction: A perspective on freshwater fluxes,  
813 convection, nutrients and productivity in high-latitude seas. *Deep Sea Research Part II: Topical*  
814 *Studies in Oceanography*, **54 (23-26)**, 2578–2598, <https://doi.org/10.1016/j.dsr2.2007.08.018>.
- 815 Carmack, E. C., and Coauthors, 2016: Freshwater and its role in the Arctic Marine System:  
816 Sources, disposition, storage, export, and physical and biogeochemical consequences in the  
817 Arctic and global oceans. *Journal of Geophysical Research G: Biogeosciences*, **121 (3)**, 675–  
818 717, <https://doi.org/10.1002/2015JG003140>.
- 819 Cohen, J., and Coauthors, 2020: Divergent consensus on Arctic amplification influence on  
820 midlatitude severe winter weather. *Nature Climate Change*, **10 (1)**, 20–29, [https://doi.org/10.](https://doi.org/10.1038/s41558-019-0662-y)  
821 [1038/s41558-019-0662-y](https://doi.org/10.1038/s41558-019-0662-y).
- 822 Cornish, S. B., Y. Kostov, H. L. Johnson, and C. Lique, 2020: Response of Arctic freshwater  
823 to the Arctic Oscillation in coupled climate models. *Journal of Climate*, **33 (7)**, 2533–2555,  
824 <https://doi.org/10.1175/JCLI-D-19-0685.1>.
- 825 Danabasoglu, G., and Coauthors, 2020: The Community Earth System Model Version 2 (CESM2).  
826 *Journal of Advances in Modeling Earth Systems*, **12 (2)**, e2019MS001916, [https://doi.org/](https://doi.org/10.1029/2019MS001916)  
827 [10.1029/2019MS001916](https://doi.org/10.1029/2019MS001916).
- 828 Davis, P. E. D., C. Lique, H. L. Johnson, and J. D. Guthrie, 2016: Competing effects of elevated  
829 vertical mixing and increased freshwater input on the stratification and sea ice cover in a  
830 changing Arctic Ocean. *Journal of Physical Oceanography*, **46 (5)**, 1531–1553, [https://doi.org/](https://doi.org/10.1175/JPO-D-15-0174.1)  
831 <https://doi.org/10.1175/JPO-D-15-0174.1>.
- 832 Davy, R., and S. Outten, 2020: The Arctic Surface Climate in CMIP6: Status and De-  
833 velopments since CMIP5. *Journal of Climate*, **33 (18)**, 8047–8068, [https://doi.org/10.1175/](https://doi.org/10.1175/JCLI-D-19-0990.1)  
834 [JCLI-D-19-0990.1](https://doi.org/10.1175/JCLI-D-19-0990.1).
- 835 Döscher, R., and Coauthors, 2021: The EC-earth3 Earth system model for the climate model  
836 intercomparison project 6. *Geoscientific Model Development Discussions*, 1–90, [https://doi.org/](https://doi.org/10.5194/gmd-2020-446)  
837 [10.5194/gmd-2020-446](https://doi.org/10.5194/gmd-2020-446).

838 Dunne, J. P., and Coauthors, 2020: The GFDL Earth System Model Version 4.1 (GFDL-ESM  
839 4.1): Overall Coupled Model Description and Simulation Characteristics. *Journal of Advances  
840 in Modeling Earth Systems*, **12** (11), e2019MS002 015, <https://doi.org/10.1029/2019MS002015>.

841 Eyring, V., S. Bony, G. A. Meehl, C. A. Senior, B. Stevens, R. J. Stouffer, and K. E. Taylor,  
842 2016: Overview of the Coupled Model Intercomparison Project Phase 6 (CMIP6) experimental  
843 design and organization. *Geoscientific Model Development*, **9** (5), 1937–1958, [https://doi.org/  
844 10.5194/gmd-9-1937-2016](https://doi.org/10.5194/gmd-9-1937-2016).

845 Giles, K. a., S. W. Laxon, A. L. Ridout, D. J. Wingham, and S. Bacon, 2012: Western Arctic Ocean  
846 freshwater storage increased by wind-driven spin-up of the Beaufort Gyre. *Nature Geoscience*,  
847 **5** (3), 194–197, <https://doi.org/10.1038/ngeo1379>.

848 Gorshkov, S. G., 1980: Atlas of Oceans. Arctic Ocean. *Minist. of Def. of the USSR, Moscow*.

849 Haine, T. W., and Coauthors, 2015: Arctic freshwater export: Status, mechanisms, and prospects.  
850 *Global and Planetary Change*, **125**, 13–35, <https://doi.org/10.1016/j.gloplacha.2014.11.013>.

851 Haine, T. W. N., 2020: Arctic Ocean Freshening Linked to Anthropogenic Climate Change:  
852 All Hands on Deck. *Geophysical Research Letters*, **47** (22), e2020GL090 678, [https://doi.org/  
853 10.1029/2020GL090678](https://doi.org/10.1029/2020GL090678).

854 Held, I. M., and B. J. Soden, 2006: Robust responses of the hydrological cycle to global warming.  
855 *Journal of climate*, **19** (21), 5686–5699, <https://doi.org/10.1175/JCLI3990.1>.

856 Heuzé, C., 2021: Antarctic Bottom Water and North Atlantic Deep Water in CMIP6 models. *Ocean  
857 Science*, **17** (1), 59–90, <https://doi.org/10.5194/os-17-59-2021>.

858 Heuzé, C., H. Zanowski, S. Karam, and M. Muilwijk, 2022: The deep Arctic Ocean and Fram  
859 Strait in CMIP6 models. *In review at Journal of Climate*.

860 Holland, M. M., J. Finnis, A. P. Barrett, and M. C. Serreze, 2007: Projected changes in Arctic  
861 Ocean freshwater budgets. *Journal of Geophysical Research: Biogeosciences*, **112** (G4), n/a–n/a,  
862 <https://doi.org/10.1029/2006JG000354>.

863 Holmes, R. M., and Coauthors, 2012: Seasonal and Annual Fluxes of Nutrients and Organic  
864 Matter from Large Rivers to the Arctic Ocean and Surrounding Seas. *Estuaries and Coasts*,  
865 **35** (2), 369–382, <https://doi.org/10.1007/s12237-011-9386-6>.

866 Ilicak, M., and Coauthors, 2016: An assessment of the Arctic Ocean in a suite of interannual CORE-  
867 II simulations. Part III: Hydrography and fluxes. *Ocean Modelling*, **100**, 141–161, <https://doi.org/10.1016/j.ocemod.2016.02.004>.

869 IPCC, 2021: *Climate Change 2021: The Physical Science Basis. Contribution of Working Group*  
870 *I to the Sixth Assessment Report of the Intergovernmental Panel on Climate Change*. Cambridge  
871 University Press.

872 Jahn, A., and R. Laiho, 2020: Forced Changes in the Arctic Freshwater Budget Emerge in the  
873 Early 21st Century. *Geophysical Research Letters*, **47** (15), e2020GL088854, <https://doi.org/10.1029/2020GL088854>.

875 Kattsov, V. M., J. E. Walsh, W. L. Chapman, V. A. Govorkova, T. V. Pavlova, and X. Zhang,  
876 2007: Simulation and Projection of Arctic Freshwater Budget Components by the IPCC AR4  
877 Global Climate Models. *Journal of Hydrometeorology*, **8** (3), 571–589, <https://doi.org/10.1175/JHM575.1>.

879 Kelley, M., and Coauthors, 2020: GISS-E2.1: Configurations and Climatology. *Journal of*  
880 *Advances in Modeling Earth Systems*, **12** (8), e2019MS002025, <https://doi.org/10.1029/2019MS002025>.

882 Khosravi, N., Q. Wang, N. Koldunov, C. Hinrichs, T. Semmler, S. Danilov, and T. Jung, 2022: The  
883 Arctic Ocean in CMIP6 Models: Biases and Projected Changes in Temperature and Salinity.  
884 *Earth's Future*, **10** (2), e2021EF002282, <https://doi.org/10.1029/2021EF002282>.

885 Li, G., L. Cheng, J. Zhu, K. E. Trenberth, M. E. Mann, and J. P. Abraham, 2020: Increasing  
886 ocean stratification over the past half-century. *Nature Climate Change*, **10** (12), 1116–1123,  
887 <https://doi.org/10.1038/s41558-020-00918-2>.

888 Lique, C., H. L. Johnson, and Y. Plancherel, 2018: Emergence of deep convection in the Arctic  
889 Ocean under a warming climate. *Climate Dynamics*, **50** (9), 3833–3847, <https://doi.org/https://doi.org/10.1007/s00382-017-3849-9>.

890

- 891 Lurton, T., and Coauthors, 2020: Implementation of the CMIP6 Forcing Data in the IPSL-  
892 CM6A-LR Model. *Journal of Advances in Modeling Earth Systems*, **12** (4), e2019MS001940,  
893 <https://doi.org/10.1029/2019MS001940>.
- 894 McDougall, T. J., and P. M. Barker, 2011: *Getting started with TEOS-10 and the Gibbs Seawater*  
895 *(GSW) Oceanographic Toolbox*. SCOR/IAPSO, 28 pp., URL [www.TEOS-10.org](http://www.TEOS-10.org).
- 896 Metzner, E. P., M. Salzmann, and R. Gerdes, 2020: Arctic Ocean Surface Energy Flux and the Cold  
897 Halocline in Future Climate Projections. *Journal of Geophysical Research: Oceans*, **125** (2),  
898 e2019JC015554, <https://doi.org/10.1029/2019JC015554>.
- 899 Muilwijk, M., and Coauthors, 2019: Arctic Ocean Response to Greenland Sea Wind Anomalies in  
900 a Suite of Model Simulations. *Journal of Geophysical Research: Oceans*, **124** (8), 6286–6322,  
901 <https://doi.org/10.1029/2019JC015101>.
- 902 Müller, W. A., and Coauthors, 2018: A Higher-resolution Version of the Max Planck Institute  
903 Earth System Model (MPI-ESM1.2-HR). *Journal of Advances in Modeling Earth Systems*,  
904 **10** (7), 1383–1413, <https://doi.org/10.1029/2017MS001217>.
- 905 Nansen, F., 1902: *The oceanography of the north polar basin*, Vol. 3. Longmans, Green, and  
906 Company.
- 907 Nguyen, a. T., D. Menemenlis, and R. Kwok, 2009: Improved modeling of the Arctic halocline with  
908 a subgrid-scale brine rejection parameterization. *Journal of Geophysical Research*, **114** (C11),  
909 C11014, <https://doi.org/10.1029/2008JC005121>.
- 910 Notz, D., and T. SIMIP Community, 2020: Arctic Sea Ice in CMIP6. *Geophysical Research Letters*,  
911 **47** (10), e2019GL086749, <https://doi.org/10.1029/2019GL086749>.
- 912 Nummelin, A., M. Ilicak, C. Li, and L. H. Smedsrud, 2016: Consequences of future increased  
913 Arctic runoff on Arctic Ocean stratification, circulation, and sea ice cover. *Journal of Geophysical*  
914 *Research: Oceans*, **121** (1), 617–637, <https://doi.org/10.1002/2015JC011156>.
- 915 Nummelin, A., C. Li, and L. H. Smedsrud, 2015: Response of Arctic Ocean stratification to  
916 changing river runoff in a column model. *Journal of Geophysical Research: Oceans*, **120** (4),  
917 2655–2675, <https://doi.org/10.1002/2014JC010571>.

- 918 Onarheim, I. H., T. Eldevik, M. Årthun, R. B. Ingvaldsen, and L. H. Smedsrud, 2015: Skill-  
919 ful prediction of Barents Sea ice cover. *Geophysical Research Letters*, **42** (13), 5364–5371,  
920 <https://doi.org/10.1002/2015GL064359>.
- 921 O’Neill, B. C., and Coauthors, 2016: The Scenario Model Intercomparison Project (ScenarioMIP)  
922 for CMIP6. *Geosci. Model Dev.*, **9** (9), 3461–3482, <https://doi.org/10.5194/gmd-9-3461-2016>.
- 923 Peralta-Ferriz, C., and R. A. Woodgate, 2015: Seasonal and interannual variability of pan-Arctic  
924 surface mixed layer properties from 1979 to 2012 from hydrographic data, and the dominance of  
925 stratification for multiyear mixed layer depth shoaling. *Progress in Oceanography*, **134**, 19–53,  
926 <https://doi.org/10.1016/j.pocean.2014.12.005>.
- 927 Peterson, B. J., R. M. Holmes, J. W. McClelland, C. J. V<sup>o</sup>r<sup>o</sup>smarty, R. B. Lammers, A. I.  
928 Shiklomanov, I. A. Shiklomanov, and S. Rahmstorf, 2002: Increasing River Discharge to the  
929 Arctic Ocean. *Science*, **298** (5601), 2171–2173, <https://doi.org/10.1126/science.1077445>.
- 930 Polyakov, I. V., A. V. Pnyushkov, and E. C. Carmack, 2018: Stability of the arctic halocline: A  
931 new indicator of arctic climate change. *Environmental Research Letters*, **13** (12), <https://doi.org/10.1088/1748-9326/aaec1e>.
- 933 Polyakov, I. V., and Coauthors, 2017: Greater role for Atlantic inflows on sea-ice loss in the  
934 Eurasian Basin of the Arctic Ocean. *Science*, **291** (April), 285–291, <https://doi.org/10.1126/science.aai8204>.
- 936 Polyakov, I. V., and Coauthors, 2020a: Borealization of the Arctic Ocean in Response to Anomalous  
937 Advection From Sub-Arctic Seas. *Frontiers in Marine Science*, **7**, <https://doi.org/10.3389/fmars.2020.00491>.
- 939 Polyakov, I. V., and Coauthors, 2020b: Weakening of Cold Halocline Layer Exposes Sea Ice  
940 to Oceanic Heat in the Eastern Arctic Ocean. *Journal of Climate*, **33** (18), 8107–8123,  
941 <https://doi.org/10.1175/JCLI-D-19-0976.1>.
- 942 Proshutinsky, a., 2002: The role of the Beaufort Gyre in Arctic climate variability: Seasonal to  
943 decadal climate scales. *Geophysical Research Letters*, **29** (23), 2100, <https://doi.org/10.1029/2002GL015847>.
- 944



- 945 Proshutinsky, A., and Coauthors, 2009: Beaufort Gyre freshwater reservoir: State and variability  
946 from observations. *Journal of Geophysical Research*, **114**, C00A10, [https://doi.org/10.1029/](https://doi.org/10.1029/2008JC005104)  
947 2008JC005104.
- 948 Proshutinsky, A., and Coauthors, 2019: Analysis of the Beaufort Gyre freshwater content in  
949 2003–2018. *Journal of Geophysical Research: Oceans*, **124** (12), 9658–9689, [https://doi.org/](https://doi.org/10.1029/2019JC015281)  
950 10.1029/2019JC015281.
- 951 Rabe, B., and Coauthors, 2011: An assessment of Arctic Ocean freshwater content changes from  
952 the 1990s to the 2006–2008 period. *Deep Sea Research Part I: Oceanographic Research Papers*,  
953 **58** (2), 173–185, <https://doi.org/10.1016/j.dsr.2010.12.002>.
- 954 Rabe, B., and Coauthors, 2014: Arctic Ocean basin liquid freshwater storage trend 1992–2012.  
955 *Geophysical Research Letters*, **41** (3), 961–968, <https://doi.org/10.1002/2013GL058121>.
- 956 Rabe, B., and Coauthors, 2022: Overview of the MOSAiC expedition: Physical oceanography.  
957 *Elementa: Science of the Anthropocene*, **10** (1), 62, [https://doi.org/10.1525/elementa.2021.](https://doi.org/10.1525/elementa.2021.00062)  
958 00062.
- 959 Randelhoff, A., J. Holding, M. Janout, M. K. Sejr, M. Babin, J.-E. Tremblay, and M. B. Alkire,  
960 2020: Pan-Arctic Ocean Primary Production Constrained by Turbulent Nitrate Fluxes. *Frontiers*  
961 *in Marine Science*, **7**, <https://doi.org/10.3389/fmars.2020.00150>.
- 962 Rosenblum, E., R. Fajber, J. C. Stroeve, S. T. Gille, L. B. Tremblay, and E. C. Carmack, 2021:  
963 Surface salinity under transitioning ice cover in the Canada Basin: Climate model biases linked  
964 to vertical distribution of fresh water. *Geophysical Research Letters*, **48** (21), e2021GL094739,  
965 <https://doi.org/https://doi.org/10.1029/2021GL094739>.
- 966 Rudels, B., 2015: Arctic Ocean circulation, processes and water masses: A description of ob-  
967 servations and ideas with focus on the period prior to the International Polar Year 2007-2009.  
968 *Progress in Oceanography*, **132**, 22–67, <https://doi.org/10.1016/j.pocean.2013.11.006>.
- 969 Rudels, B., E. P. Jones, U. Schauer, and P. Eriksson, 2004: Atlantic sources of the Arc-  
970 tic Ocean surface and halocline waters. *Polar Research*, **23** (2), 181–208, [https://doi.org/](https://doi.org/10.1111/j.1751-8369.2004.tb00007.x)  
971 10.1111/j.1751-8369.2004.tb00007.x.

972 Seland, O., and Coauthors, 2020: The Norwegian Earth System Model, NorESM2 – Evaluation  
973 of the CMIP6 DECK and historical simulations. *Geoscientific Model Development Discussions*,  
974 **13 (February)**, 1–68, <https://doi.org/10.5194/gmd-2019-378>.

975 Sellar, A. A., and Coauthors, 2020: Implementation of U.K. Earth System Models for CMIP6.  
976 *Journal of Advances in Modeling Earth Systems*, **12 (4)**, e2019MS001946, [https://doi.org/](https://doi.org/10.1029/2019MS001946)  
977 [10.1029/2019MS001946](https://doi.org/10.1029/2019MS001946).

978 Serreze, M. C., and Coauthors, 2006: The large-scale freshwater cycle of the Arctic. *Journal of*  
979 *Geophysical Research*, **111 (C11)**, <https://doi.org/10.1029/2005JC003424>.

980 Shen, Z., A. Duan, D. Li, and J. Li, 2021: Assessment and Ranking of Climate Models in Arctic  
981 Sea Ice Cover Simulation: From CMIP5 to CMIP6. *Journal of Climate*, **34 (9)**, 3609–3627,  
982 <https://doi.org/10.1175/JCLI-D-20-0294.1>.

983 Shepherd, A., and Coauthors, 2020: Mass balance of the Greenland Ice Sheet from 1992 to 2018.  
984 *Nature*, **579 (7798)**, 233–239, <https://doi.org/https://doi.org/10.1038/s41586-019-1855-2>.

985 Shu, Q., F. Qiao, Z. Song, J. Zhao, and X. Li, 2018: Projected freshening of the Arctic Ocean in the  
986 21st century. *Journal of Geophysical Research: Oceans*, **123 (12)**, 9232–9244, [https://doi.org/](https://doi.org/https://doi.org/10.1029/2018JC014036)  
987 <https://doi.org/10.1029/2018JC014036>.

988 Shu, Q., Q. Wang, Z. Song, F. Qiao, J. Zhao, M. Chu, and X. Li, 2020: Assessment of sea ice  
989 extent in CMIP6 with comparison to observations and CMIP5. *Geophysical Research Letters*,  
990 **47 (9)**, e2020GL087965, <https://doi.org/10.1029/2020GL087965>.

991 Shu, Q., Q. Wang, J. Su, X. Li, and F. Qiao, 2019: Assessment of the Atlantic water layer in the  
992 Arctic Ocean in CMIP5 climate models. *Climate Dynamics*, **53 (9)**, 5279–5291, [https://doi.org/](https://doi.org/10.1007/s00382-019-04870-6)  
993 [10.1007/s00382-019-04870-6](https://doi.org/10.1007/s00382-019-04870-6).

994 Smedsrud, L. H., and Coauthors, 2022: Nordic Seas Heat Loss, Atlantic Inflow, and Arctic Sea Ice  
995 Cover Over the Last Century. *Reviews of Geophysics*, **60 (1)**, e2020RG000725, [https://doi.org/](https://doi.org/10.1029/2020RG000725)  
996 [10.1029/2020RG000725](https://doi.org/10.1029/2020RG000725).

997 Solomon, A., and Coauthors, 2021: Freshwater in the Arctic Ocean 2010–2019. *Ocean Science*,  
998 **17 (4)**, 1081–1102, <https://doi.org/10.5194/os-17-1081-2021>.

- 999 Steele, M., 2004: Circulation of summer Pacific halocline water in the Arctic Ocean. *Journal of*  
1000 *Geophysical Research*, **109** (C2), <https://doi.org/10.1029/2003JC002009>, URL <http://doi.wiley.com/10.1029/2003JC002009>.  
1001
- 1002 Steele, M., G. L. Mellor, and M. G. Mcphee, 1989: Role of the Molecular Sublayer in the Melting  
1003 or Freezing of Sea Ice. *Journal of Physical Oceanography*, **19** (1), 139–147, [https://doi.org/10.1175/1520-0485\(1989\)019<0139:ROTMSI>2.0.CO;2](https://doi.org/10.1175/1520-0485(1989)019<0139:ROTMSI>2.0.CO;2).  
1004
- 1005 Stroeve, J., and D. Notz, 2018: Changing state of Arctic sea ice across all seasons. *Environmental*  
1006 *Research Letters*, **13** (10), 103 001, <https://doi.org/10.1088/1748-9326/aade56>.
- 1007 Swart, N. C., and Coauthors, 2019: The Canadian Earth System Model version 5  
1008 (CanESM5.0.3). *Geoscientific Model Development*, **12** (11), 4823–4873, <https://doi.org/10.5194/gmd-12-4823-2019>.  
1009
- 1010 Tailleux, R., 2009: Understanding mixing efficiency in the oceans: do the nonlinearities of  
1011 the equation of state for seawater matter? *Ocean Science*, **5** (3), 271–283, <https://doi.org/10.5194/os-5-271-2009>.  
1012
- 1013 Tatebe, H., and Coauthors, 2019: Description and basic evaluation of simulated mean state, internal  
1014 variability, and climate sensitivity in MIROC6. *Geoscientific Model Development*, **12** (7), 2727–  
1015 2765, <https://doi.org/10.5194/gmd-12-2727-2019>.
- 1016 Timmermans, M. L., and J. Marshall, 2020: Understanding Arctic Ocean Circulation: A Review  
1017 of Ocean Dynamics in a Changing Climate. *Journal of Geophysical Research: Oceans*, **125** (4),  
1018 1–70, <https://doi.org/10.1029/2018JC014378>.
- 1019 Timokhov, L., and F. Tanis, 1997: Environmental Working Group Joint U.S.-Russian Atlas of the  
1020 Arctic Ocean, Version 1. <https://doi.org/10.7265/N5H12ZX4>.
- 1021 Treshnikov, A. F., 1985: Arctic atlas. *Head Administration of Geodesy and Cartography of the*  
1022 *Soviet Ministry, Moscow*, 204.
- 1023 Tsubouchi, T., K. Våge, B. Hansen, K. M. H. Larsen, S. Østerhus, C. Johnson, S. Jónsson,  
1024 and H. Valdimarsson, 2021: Increased ocean heat transport into the Nordic Seas and Arctic

- 1025 Ocean over the period 1993–2016. *Nature Climate Change*, **11** (1), 21–26, [https://doi.org/](https://doi.org/10.1038/s41558-020-00941-3)  
1026 10.1038/s41558-020-00941-3.
- 1027 Tsujino, H., and Coauthors, 2020: Evaluation of global ocean–sea-ice model simulations based on  
1028 the experimental protocols of the Ocean Model Intercomparison Project phase 2 (OMIP-2). *Geo-*  
1029 *scientific Model Development*, **13** (8), 3643–3708, <https://doi.org/10.5194/gmd-13-4595-2020>.
- 1030 Wang, Q., J. Marshall, J. Scott, G. Meneghello, S. Danilov, and T. Jung, 2019: On the Feedback  
1031 of Ice–Ocean Stress Coupling from Geostrophic Currents in an Anticyclonic Wind Regime  
1032 over the Beaufort Gyre. *Journal of Physical Oceanography*, **49** (2), 369–383, [https://doi.org/](https://doi.org/10.1175/JPO-D-18-0185.1)  
1033 10.1175/JPO-D-18-0185.1.
- 1034 Wang, Q., and Coauthors, 2016: An assessment of the Arctic Ocean in a suite of interannual  
1035 CORE-II simulations. Part II: Liquid freshwater. *Ocean Modelling*, **99**, 86–109, [https://doi.org/](https://doi.org/10.1016/j.ocemod.2015.12.009)  
1036 10.1016/j.ocemod.2015.12.009.
- 1037 Wang, S., Q. Wang, M. Wang, G. Lohmann, and F. Qiao, 2021: Arctic Ocean liquid freshwater  
1038 in CMIP6 coupled models. *Earth and Space Science Open Archive ESSOAr*, [https://doi.org/](https://doi.org/10.1002/essoar.10505861.1)  
1039 10.1002/essoar.10505861.1.
- 1040 Woodgate, R. a., K. Aagaard, J. H. Swift, K. K. Falkner, and W. M. Smethie, 2005: Pacific ventila-  
1041 tion of the Arctic Ocean’s lower halocline by upwelling and diapycnal mixing over the continental  
1042 margin. *Geophysical Research Letters*, **32** (18), <https://doi.org/10.1029/2005GL023999>.
- 1043 Woodgate, R. a., T. J. Weingartner, and R. Lindsay, 2012: Observed increases in Bering Strait  
1044 oceanic fluxes from the Pacific to the Arctic from 2001 to 2011 and their impacts on the  
1045 Arctic Ocean water column. *Geophysical Research Letters*, **39** (24), [https://doi.org/10.1029/](https://doi.org/10.1029/2012GL054092)  
1046 2012GL054092.
- 1047 Wu, T., and Coauthors, 2019: The Beijing Climate Center Climate System Model (BCC-CSM): the  
1048 main progress from CMIP5 to CMIP6. *Geoscientific Model Development*, **12** (4), 1573–1600,  
1049 <https://doi.org/10.5194/gmd-12-1573-2019>.
- 1050 Xin-Yao, R., L. I. Jian, C. Hao-Ming, X. I. N. Yu-Fei, S. U. Jing-Zhi, and H. U. A. Li-Juan, 2019:  
1051 Introduction of CAMS-CSM model and its participation in CMIP6. *Advances in Climate Change*  
1052 *Research*, **15** (5), 540, <https://doi.org/10.12006/j.issn.1673-1719.2019.186>.

- 1053 Yasunaka, S., and Coauthors, 2018: Arctic Ocean CO<sub>2</sub> uptake: an improved multiyear estimate  
1054 of the air-sea CO<sub>2</sub> flux incorporating chlorophyll a concentrations. *Biogeosciences*, **15** (6),  
1055 1643–1661, <https://doi.org/10.5194/bg-15-1643-2018>, URL [https://bg.copernicus.org/articles/](https://bg.copernicus.org/articles/15/1643/2018/)  
1056 [15/1643/2018/](https://bg.copernicus.org/articles/15/1643/2018/).
- 1057 Yukimoto, S., and Coauthors, 2019: The Meteorological Research Institute Earth System Model  
1058 Version 2.0, MRI-ESM2.0: Description and Basic Evaluation of the Physical Component.  
1059 *Journal of the Meteorological Society of Japan. Ser. II*, **97** (5), 931–965, [https://doi.org/10.](https://doi.org/10.2151/jmsj.2019-051)  
1060 [2151/jmsj.2019-051](https://doi.org/10.2151/jmsj.2019-051).
- 1061 Zanowski, H., A. Jahn, and M. M. Holland, 2021: Arctic Ocean Freshwater in CMIP6 Ensembles:  
1062 Declining Sea Ice, Increasing Ocean Storage and Export. *Journal of Geophysical Research:*  
1063 *Oceans*, **126** (4), e2020JC016930, <https://doi.org/10.1029/2020JC016930>.